GENETICS

Mitochondrial protein-linked DNA breaks perturb mitochondrial gene transcription and trigger free radical–induced DNA damage

Shih-Chieh Chiang,[1] Martin Meagher,[2] Nick Kassouf,[3] Majid Hafezparast,[4] Peter J. McKinnon,[5] Rachel Haywood,[3] Sherif F. El-Khamisy[1,6]*

Breakage of one strand of DNA is the most common form of DNA damage. Most damaged DNA termini require end-processing in preparation for ligation. The importance of this step is highlighted by the association of defects in the 3′-end processing enzyme tyrosyl DNA phosphodiesterase 1 (TDP1) and neurodegeneration and by the cytotoxic induction of protein-linked DNA breaks (PDBs) and oxidized nucleic acid intermediates during chemotherapy and radiotherapy. Although much is known about the repair of PDBs in the nucleus, little is known about this process in the mitochondria. We reveal that TDP1 resolves mitochondrial PDBs (mtPDBs), thereby promoting mitochondrial gene transcription. Overexpression of a toxic form of mitochondrial topoisomerase I (TOP1mt*), which generates excessive mtPDBs, results in a TDP1-dependent compensatory upregulation of mitochondrial gene transcription. In the absence of TDP1, the imbalance in transcription of mitochondrial- and nuclear-encoded electron transport chain (ETC) subunits results in misassembly of ETC complex III. Bioenergetics profiling further reveals that TDP1 promotes oxidative phosphorylation under both basal and high energy demands. It is known that mitochondrial dysfunction results in free radical leakage and nuclear DNA damage; however, the detection of intermediates of radical damage to DNA is yet to be shown. Consequently, we report an increased accumulation of carbon-centered radicals in cells lacking TDP1, using electron spin resonance spectroscopy. Overexpression of the antioxidant enzyme superoxide dismutase 1 (SOD1) reduces carbon-centered adducts and protects TDP1-deficient cells from oxidative stress. Conversely, overexpression of the amyotrophic lateral sclerosis–associated mutant $SOD1^{G93A}$ leads to marked sensitivity. Whereas Tdp1 knockout mice develop normally, overexpression of $SOD1^{G93A}$ suggests early embryonic lethality. Together, our data show that TDP1 resolves mtPDBs, thereby regulating mitochondrial gene transcription and oxygen consumption by oxidative phosphorylation, thus conferring cellular protection against reactive oxygen species–induced damage.

INTRODUCTION

As aerobic organisms, our cells and genetic materials are under constant exposure to toxic metabolites of respiration. The ability to detect and repair free radical–induced damage is critical to maintaining the structural and functional integrity of cells. Failure in this response can result in mutagenesis, inhibition of transcription, organelle dysfunction, and cell death. Almost all DNA termini produced by endogenous or exogenous sources of DNA damage lack the conventional chemistries required for DNA ligation (3′-OH and 5′-PO_4). Therefore, nature has evolved a number of DNA end-processing enzymes to clean up damaged DNA termini. Tyrosyl DNA phosphodiesterase 1 (TDP1) is a broad-spectrum DNA end-processing enzyme that deals with a variety of 3′-damaged termini, including oxidized sugar/base fragments and TOP1 peptides (*1*–*8*). Progressive accumulation of unprocessed TDP1 substrates causes neurodegeneration in humans, and their acute accumulation has been used to improve anticancer and antiviral therapies (*5*, *9*–*17*).

The neuroprotective role of TDP1 has been primarily attributed to its nuclear DNA repair function, but its role in the mitochondria is less well understood. In cultured mammalian cells, TDP1 has been shown to localize to the mitochondria, with putative roles in mitochondrial DNA (mtDNA) replication following oxidative DNA damage (*18*–*20*). The mitochondria play a pivotal role in the health of neuronal cells by providing vital energy and metabolizing macromolecules throughout the life span of cells. Reactive oxygen species (ROS) generated in the mitochondria is an unavoidable by-product, which, if allowed to accumulate, leads to a vicious cycle of mitochondrial dysfunction, leading to more ROS production. Recent elegant studies have nicely shown the importance of mitochondrial TOP1 (TOP1mt) in mitochondrial gene transcription (*21*) and replication (*22*, *23*) and in maintaining mitochondrial function (*22*–*24*). Similar to its nuclear counterpart, TOP1mt removes negative and positive supercoils generated during DNA transactions (*25*–*27*) and may potentially become trapped in the vicinity of modified DNA bases (*28*–*33*). However, how mammalian mitochondria resolve these lesions and their consequence on mitochondrial and cellular function remains to be tested (*34*). Here, we report that TDP1 is able to resolve mitochondrial TOP1-linked DNA breaks and functionally interacts with TOP1mt to regulate mitochondrial gene transcription, electron transport chain (ETC) complex III assembly, and oxygen consumption, thereby conferring cellular protection against ROS-induced damage.

RESULTS

To examine the putative role of TDP1 during mtDNA repair, we generated a doxycycline-inducible knockdown cell line and an isogenic

[1]Krebs Institute and Sheffield Institute for Nucleic Acids, Department of Molecular Biology and Biotechnology, Firth Court, University of Sheffield, S10 2TN Sheffield, U.K. [2]Wellcome Trust Centre for Mitochondrial Research, Medical School, Newcastle University, Framlington Place, Newcastle upon Tyne NE2 4HH, U.K. [3]RAFT Institute, Mount Vernon Hospital, Northwood, Middlesex HA6 2RN, U.K. [4]School of Life Sciences, University of Sussex, Brighton BN1 9QG, U.K. [5]Department of Genetics, St. Jude Children's Research Hospital, Memphis, TN 38105–3678, USA. [6]Center for Genomics, Helmy Institute for Medical Sciences, Zewail City of Science and Technology, Giza 12588, Egypt.
*Corresponding author. Email: s.el-khamisy@sheffield.ac.uk

control complemented with RNA interference (RNAi)–resistant human TDP1 (hTDP1) (fig. S1A). We first confirmed efficient TDP1 depletion using a biochemical activity assay with fluorophore-labeled TDP1 substrates (fig. S1B), an alkaline comet assay measuring the accumulation of camptothecin (CPT)–induced TOP1 breaks (fig. S1C), and CPT survival assays (fig. S1D). We then engineered an inducible system whereby depletion of TDP1 is simultaneously achieved with the expression of either wild-type (WT) TOP1mt or a version harboring the T554A/N558H mutation (TOP1mt*), which specifically induces mitochondrial protein-linked DNA breaks (mtPDBs) by inhibiting the DNA religation activity of TOP1mt (Fig. 1A) (*33*). Overexpression of TOP1mt* has advantages over topoisomerase poisons such as CPT, which also target the nuclear genome and have limited mitochondrial permeability and activity due to the alkaline nature of the mitochondrial matrix (*25*, *34*–*37*).

To assess the extent of mtPDBs generated by overexpression of TOP1mt and TOP1mt*, we purified TOP1mt DNA cleavage complexes (TOP1mt-cc) from mitochondrial extracts using cesium chloride fractionation and antibodies against green fluorescent protein (GFP) to detect TOP1mt-GFP– and TOP1mt*-GFP–linked DNA breaks.

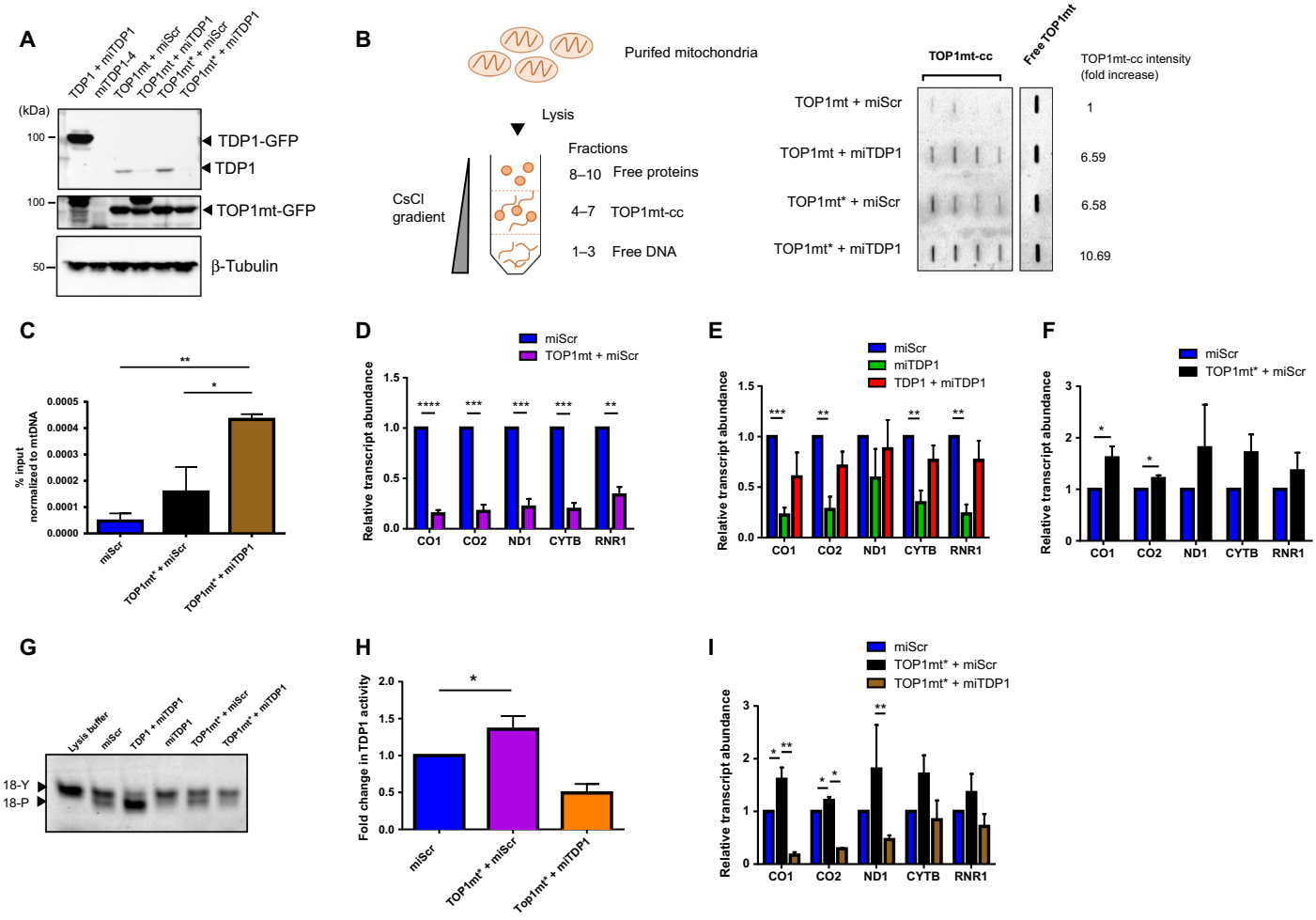

Fig. 1. TDP1 promotes mitochondrial gene transcription in human cells. (**A**) Immunoblotting of Flp-In T-Rex 293 cell lines after doxycycline induction using antibodies against TDP1, GFP, and β tubulin. TDP1 + miTDP1, TDP1-depleted cells overexpressing microRNA (miRNA)–resistant TDP1; miTDP1-4, TDP1-depleted cells (clone 4); TOP1mt + miScr, scrambled miRNA–transfected cells overexpressing TOP1mt-EmGFP; TOP1mt + miTDP1, miTDP1 cells overexpressing TOP1mt-EmGFP; TOP1mt* + miScr, miScr cells overexpressing TOP1mt^{T554A,N558H}-EmGFP; TOP1mt* + miTDP1, miTDP1 cells overexpressing TOP1mt^{554A,N558H}-EmGFP. (**B**) Mitochondrial lysates from doxycycline-induced cells were fractionated using CsCl gradient and immunoblotted using antibodies against GFP to detect TOP1mt- and TOP1mt*-linked DNA breaks. Enhanced chemiluminescence intensity was quantified and expressed as fold increase relative to TOP1mt-expressing cells. (**C**) TOP1mt*-cc in doxycycline-induced cells were immunoprecipitated using GFP-trap magnetic beads and the bound mtDNA at a putative TOP1mt*-binding site in the noncoding regulatory region quantified by qPCR. The mtDNA copy numbers of each cell line were concomitantly measured using primers for the ND1 (mitochondrial) and B2M (nuclear) genes. Enrichment of TOP1mt-bound chromatin is expressed as percent input, which is then normalized to the mitochondrial copy number of the cell line. (**D** to **F** and **I**) Total RNA from doxycycline-induced cells from (A) was reverse-transcribed and analyzed by SYBR-Green–based qPCR using primers for mitochondrial-encoded genes. Mitochondrial transcript levels were normalized against glyceraldehyde-3-phosphate dehydrogenase (GAPDH) levels and expressed as a fraction against the corresponding mitochondrial gene transcript in control scrambled miRNA–transfected (miScr) cells. Data are the means of three independent experiments, and error bars represent ±1 SEM. (**G**) Mitochondrial lysates of doxycycline-induced cells were incubated with 5′-Cy5.5–labeled 18-mer substrate with a 3′-phosphotyrosine terminus (18-Y) that is processed to 3′-phosphate (18-P) by TDP1. (**H**) Quantification of product conversion normalized to miScr cells from three independent experiments described in (G) using LI-COR Image Studio Lite version 5.2. *P < 0.05; **P < 0.01; ***P < 0.001; ****P < 0.0001.

Overexpression of WT TOP1mt only resulted in a mild increase in TOP1mt-cc compared to control cells (fig. S2A), suggesting that human cells have activities required to resolve TOP1mt-linked DNA breaks. Repeating the experiment in TDP1-depleted cells revealed an approximately 6.5-fold increase in TOP1mt-cc (Fig. 1B). Overexpression of TOP1mt* induced ~6.5-fold more mtPDBs than WT TOP1mt, and TDP1 depletion further increased this by another ~1.6-fold, which is ~10.7-fold above TOP1mt overexpression alone (Fig. 1B). To confirm that the GFP signal was specific to TOP1mt-GFP and TOP1mt*-GFP, we made use of a newly developed antibody against the TOP1-DNA covalent complex, which detects the tertiary structure at the catalytic sites conserved between TOP1 and TOP1mt (*25*, *38*). Again, we observed more TOP1mt-cc in TOP1mt*-overexpressing mitochondrial extracts than TOP1mt extracts (fig. S2B). To further assess the role of TDP1 during mtPDB repair, we compared TDP1-proficient and TDP1-deficient cells for levels of TOP1mt*-bound mtDNA in the promoter-containing noncoding regulatory region, which is a known binding site for TOP1mt* (*33*). Depletion of TDP1 led to an approximately fourfold increase in TOP1mt-cc, as quantified by quantitative polymerase chain reaction (qPCR) ($P < 0.05$; Fig. 1C), which was not caused by a change in mtDNA template abundance because mtDNA copy number was comparable across the cell lines tested within each individual experiment (fig. S2C). Together, we conclude that TDP1 is capable of resolving mitochondrial TOP1-linked DNA breaks.

We then examined the role of TDP1 during mitochondrial gene transcription. We analyzed multiple sites along the polycistronic heavy-chain transcript, from the 5′-end *RNR1* gene to the 3′-end *CYTB* gene, to allow detection of primary transcripts of different lengths. In agreement with published work (*21*), overexpression of TOP1mt led to a marked reduction of the five mitochondrial mRNA transcripts examined via quantitative reverse transcription PCR (qRT-PCR) ($P < 0.001$; Fig. 1D and fig. S2D). Consistent with a role of TDP1 during mtPDB repair, depletion of TDP1 led to an approximately 50% reduction of all transcripts tested, which was partially rescued by complementation with hTDP1 ($P < 0.01$; Fig. 1E). In striking contrast to WT TOP1mt, overexpression of TOP1mt* led to an approximately twofold increase in mitochondrial gene transcription ($P < 0.05$; Fig. 1F). Given the observed role for TDP1 to process TOP1mt*-induced DNA breaks (Fig. 1B), we reasoned that the increase in transcription might be due to a compensatory up-regulation of TDP1. This was indeed the case, as shown by an approximately 25% increase in mitochondrial TDP1 catalytic activity in cells overexpressing TOP1mt* ($P < 0.05$; Fig. 1, G and H). Consistent with this, depletion of TDP1 was sufficient to abrogate the TOP1mt*-induced transcription up-regulation ($P < 0.05$; Fig. 1I).

Because transcription of mtDNA-encoded genes is essential for the synthesis of major subunits of all the ETC complexes of the OXPHOS system except complex II, we next assessed the assembly of these complexes in purified mitochondria by probing for the subunits that are particularly labile when the complexes are not correctly assembled (Fig. 2A) (*39*). As expected, neither depletion of TDP1 nor overexpression of TOP1mt* had a significant effect on the nuclear-encoded complex II subunit SDHB at both the protein and mRNA levels (Fig. 2, A and C, and fig. S3). Although we did not observe a significant reduction in the stability of complexes I, IV, and V (Fig. 2, B, E, and F), the most noticeable difference was detected with complex III, which was further confirmed by complex III–specific antibodies (Fig. 2A). When normalized to the mitochondrial structural protein VDAC1 (porin), the level of UQCRC2 in complex III was reduced by ~40% upon TDP1 depletion ($P < 0.01$; Fig. 2D). We conclude from these experiments that TDP1 promotes the integrity of the ETC complex III subunit.

Next, we examined whether the deregulation of complex III affects the OXPHOS function of the ETC complexes by measuring cellular oxygen consumption using the Seahorse Bioanalyzer. This technique monitors real-time cellular oxygen consumption rate (OCR) under basal conditions and following sequential challenges with the adenosine 5′-triphosphate (ATP) synthase inhibitor oligomycin, the mitochondrial membrane uncoupler FCCP, and the mitochondrial complex I inhibitor rotenone. Suppression of all mitochondrial respiration by rotenone and the complex III inhibitor antimycin-A allowed the definition of the baseline levels of nonmitochondrial OCR (Fig. 3A). We first examined the basal respiration of WT and TDP1-depleted cells. Consistent with its role during mitochondrial gene transcription (Fig. 1E) and complex III assembly (Fig. 2D), TDP1 depletion resulted in an approximately 25% reduction in OCR compared to WT cells ($P < 0.01$; Fig. 3B). Overexpression of TOP1mt* reduced basal respiration by ~30% ($P < 0.05$; Fig. 3C), and depletion of TDP1 in these cells had no further detectable effect on basal respiration (Fig. 3D). The lower OCRs were due to loss of ATP-coupled respiration (Fig. 3, E to G) because inhibition of ATP-coupled respiration by oligomycin revealed no significant changes in uncoupled respiration (proton leak) across the cell lines (fig. S4). Upon induction of maximal respiration by FCCP, mimicking the state of high ATP demand, TDP1-depleted cells showed ~25% lower spare respiratory capacity (SRC) compared to WT cells ($P < 0.01$; Fig. 3H). TOP1mt*-overexpressing cells had less than 25% SRC compared to control cells ($P < 0.01$; Fig. 3I). Simultaneous depletion of TDP1 partially rescued this defect to ~50% of the baseline level. Together, we conclude that TDP1 promotes OXPHOS under both basal and high energy demands.

Mitochondrial dysfunction is predicted to increase the levels of cellular free radicals, attacking both nuclear DNA and mtDNA. To examine the role of TDP1 in the cellular homeostasis of free radicals, we established vertebrate *Tdp1*$^{-/-}$ DT40 cells and isogenic lines stably expressing different levels of hTDP1. TDP1 expression was assessed by immunoblotting (Fig. 4A) and by a TDP1 enzymatic assay measuring the liberation of tyrosine from 3′-phosphotyrosine oligonucleotide substrates (Fig. 4B) (*40*). We then used electron spin resonance (ESR) spectroscopy to directly quantify the levels of carbon-centered radicals (*41*, *42*). The ESR profile was consistent with that of nucleic acids, suggesting DNA-derived carbon-centered radicals (Fig. 4C). *Tdp1*$^{-/-}$ cells displayed an approximately eightfold increase in carbon radicals compared to WT DT40 cells. The increase was TDP1-dependent because expression of hTDP1 in *Tdp1*$^{-/-}$ cells led to a significant reduction of carbon adducts ($P < 0.05$; Fig. 4D). To test whether this is an epiphenomenon of vertebrate DT40 cells, we established *Tdp1*$^{-/-}$ mouse embryonic fibroblasts (MEFs) and an isogenic control expressing hTDP1 using retroviral transduction. We first examined the protective effect of Tdp1 against oxidative free radical damage induced by H_2O_2 or ionizing radiation (IR). Consistent with previous reports using *Tdp1*$^{-/-}$ mouse astrocytes (*43*) and chicken DT40 B-lymphocytes (*13*), *Tdp1*$^{-/-}$ MEFs were significantly more sensitive to H_2O_2 and IR compared to *Tdp1*$^{-/-}$ MEFs complemented with hTDP1 ($P < 0.05$; Fig. 4, E and F). Our initial experiments revealed a consistent increase of carbon radicals in *Tdp1*$^{-/-}$ MEFs compared to controls. To examine this further, we took advantage of a pathologic mutant superoxide dismutase 1, SOD1^{G93A}, associated with amyotrophic lateral sclerosis. The toxic mutant induces high levels of

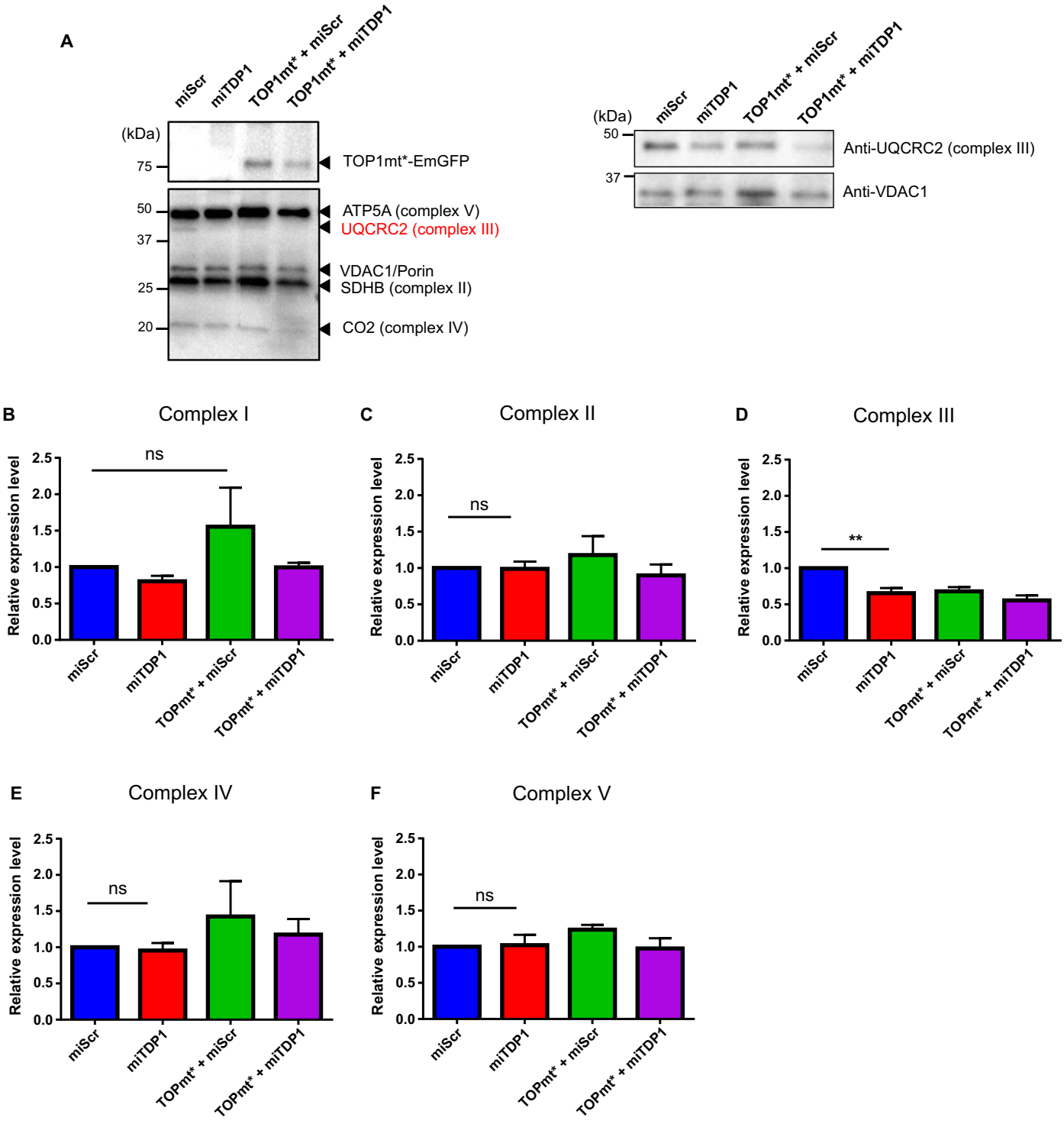

Fig. 2. TDP1 promotes the assembly of mitochondrial OXPHOS system. (**A**) Left: Immunoblotting of mitochondrial lysates from doxycycline-induced Flp-In T-Rex 293 cells using cocktail antibodies against OXPHOS proteins NDUFB8 (complex I), SDHB (complex II), UQCRC2 (complex III), COX-II (complex IV), and ATP5A (complex V). Right: Immunoblotting of mitochondrial lysates with antibodies specific to UQCRC2 (complex III) and the mitochondrial loading control VDAC1. (**B** to **F**) Protein expression levels of the labile subunit from the indicated complexes relative to those of control cells, after normalization to levels of the mitochondrial loading control VDAC1. ns, not statistically significant; $P > 0.05$.

mitochondrial ROS production through multiple mechanisms (*44*). We stably overexpressed human SOD1 or SOD1^{G93A} (hSOD1 or hSDO1^{G93A}, respectively) in *Tdp1*$^{-/-}$ MEFs by retroviral transduction (Fig. 4G) and then subjected the cell lines to ESR analyses. Again, the pattern of carbon-centered radicals corresponded to that of nucleic acid–derived radicals (Fig. 4H). Whereas *Tdp1*$^{-/-}$ cells exhibited an approximately sixfold

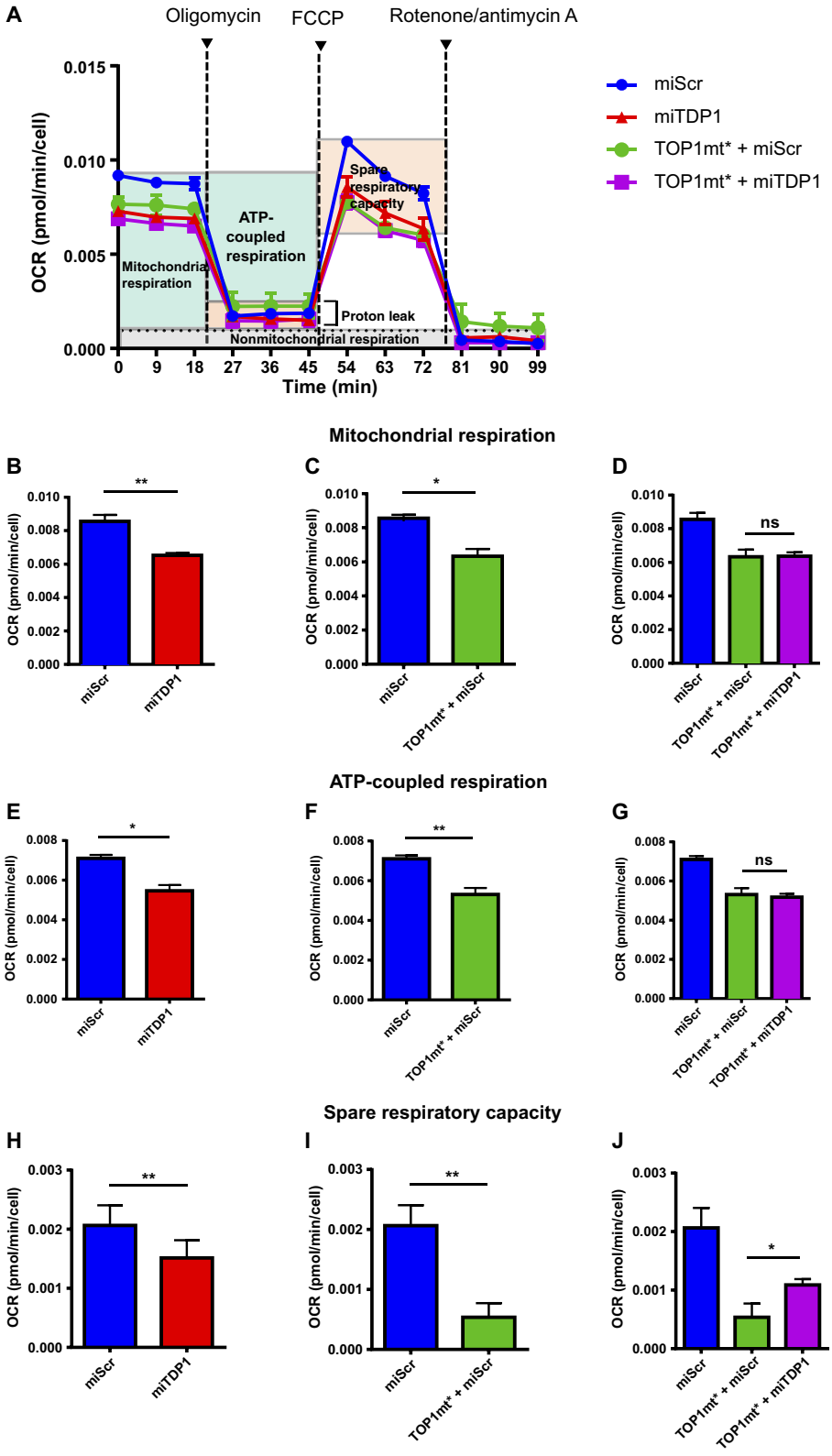

Fig. 3. TDP1 promotes OXPHOS at basal and high ATP demands. (**A**) Doxycycline-induced cells were plated in an XF24 Seahorse cell plate, and the bioenergetic response to 1 μM oligomycin, 1 μM FCCP, and 1 μM rotenone was analyzed in a Seahorse XF Bioanalyzer. Data represent the mean OCR of three independent experiments, and error bars represent ±1 SEM. (**B** to **D**) Mitochondrial respiration was calculated by subtracting OCR after rotenone/antimycin A from basal OCR. (**E** to **G**) ATP-coupled respiration was calculated by subtracting OCR after oligomycin from basal OCR. (**H** to **J**) SRC was calculated by subtracting maximum OCR after FCCP from basal OCR. Data are the means of three independent experiments, and error bars represent ±1 SEM.

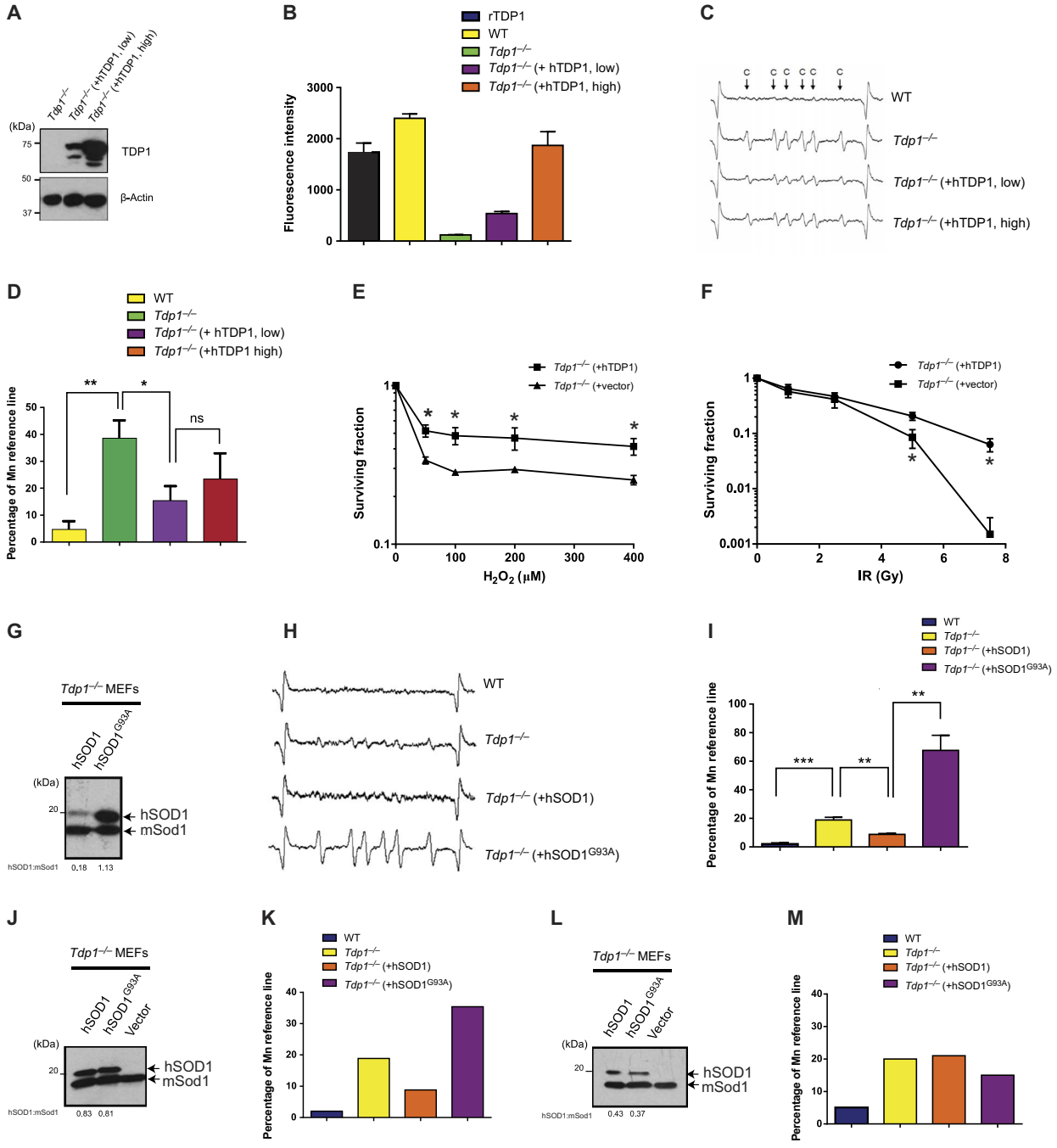

Fig. 4. Accumulation of carbon radicals in Tdp1 deficient vertebrate cells. (**A**) Immunoblotting of cell lysates from *Tdp1*$^{-/-}$ DT40 cells complemented with hTDP1 or an empty vector using antibodies against hTDP1. (**B**) TDP1 enzymatic activity measured on cell lysates from (A) using an in vitro assay with an 18-mer oligonucleotide substrate containing a 3′-phosphotyrosine residue and a fluorescein isothiocyanate (FITC) molecule conjugated to the 5′-end. Recombinant hTDP1 (rTDP1) was used as positive control. Fluorescence intensity was measured with a BMG Labtech PHERAstar plate reader and analyzed by the PHERAstar software. (**C**) ESR spectra obtained during 30 min of UVA irradiation (approximately 3.1 mW/cm^2) of DT40 cells. (**D**) Bar charts showing the mean integration of all six carbon adducts shown in (C) noted as a percentage of integrated manganese reference lines. Data are the means of three independent experiments, and error bars represent ±1 SEM. (**E** and **F**) MEFs were treated with the indicated doses of H_2O_2 for 10 min on ice or exposed to x-ray irradiation at 12 mA/250 kV on ice and then left to recover until macroscopic colonies formed. Surviving fraction was calculated by dividing the number of colonies on treated plates by the number on untreated plates. Data are the means of three independent experiments, and error bars represent ±1 SEM. (**G**) Immunoblotting of *Tdp1*$^{-/-}$ MEFs complemented with hSOD1 or hSOD1^{G93A}. Expression levels of hSOD1 and hSOD1^{G93A} were quantified by ImageJ and noted as a fraction relative to endogenous mouse Sod1 (mSod1). (**H**) ESR spectra obtained during 30 min of UVA irradiation (approximately 5 mW/cm^2) of MEFs in (G). (**I**) Bar charts showing the mean integration of all six carbon adducts from (G) noted as a percentage of integrated manganese reference lines. SEM was calculated from three independent experiments. (**J** and **L**) Immunoblotting of *Tdp1*$^{-/-}$ MEF lysates overexpressing hSOD1 or hSOD1^{G93A}. Expression levels of hSOD1 are noted as a fraction relative to endogenous mouse Sod1 (mSod1). (**K** and **M**) Bar charts showing the mean integration of all six carbon adducts noted as a percentage of integrated manganese reference lines from ESR data obtained from MEFs in (J) and (L), respectively. *P < 0.05; **P < 0.01; ***P < 0.001; ****P < 0.0001.

increase in carbon adducts compared to controls, overexpression of hSOD1 led to marked suppression ($P < 0.01$; Fig. 4I). In contrast, overexpression of $hSOD1^{G93A}$ led to an approximately twelvefold increase in carbon adducts compared to control or $Tdp1^{-/-}$ cells ($P < 0.01$; Fig. 4I). To test whether the increase in carbon adducts was dependent on $SOD1^{G93A}$ expression levels, we screened and established $Tdp1^{-/-}$ cells expressing different levels of $SOD1^{G93A}$ (Fig. 4, J and L). Reduction of the ratio of ectopic $hSOD1^{G93A}$ to endogenous SOD1 expression from 1.1 to 0.8 attenuated the increase in carbon adducts from approximately twelvefold to eightfold (Fig. 4K). Furthermore, a further reduction of the ratio of $hSOD1^{G93A}$ to endogenous Sod1 to 0.37 failed to impact on the level of carbon adducts compared to levels detected in $Tdp1^{-/-}$ cells (Fig. 4M). Together, we conclude from these experiments that TDP1 controls the level of ROS-induced carbon radicals in vertebrate cells.

To test whether the observed effects on carbon radicals correlate with nuclear chromosomal breaks, we quantified DNA single-strand breaks (SSBs) using the alkaline comet assays. For these experiments, we used a low-dose H_2O_2 (10 μM) that acts as a substrate for $SOD1^{G93A}$, which converts it to reactive hydroxyl and superoxide radicals through the Fenton reaction (*45*–*47*). After 10 min of H_2O_2 treatment, $Tdp1^{-/-}$ cells displayed approximately twofold more strand breaks than WT cells, confirming a role for TDP1 in controlling the level of free radical–induced strand breaks. Overexpression of $hSOD1^{G93A}$ in $Tdp1^{-/-}$ cells induced approximately threefold more breaks. Conversely, overexpression of hSOD1 in $Tdp1^{-/-}$ cells suppressed the observed increase in DNA strand breaks to background levels detected in WT cells ($P < 0.001$; Fig. 5A). Subsequent incubation in H_2O_2-free media led to rapid clearance of SSBs with no detectable difference in repair kinetics (Fig. 5B). We next examined the effect of modulating endogenous free radicals on cell survival. Consistent with the ESR and comet assay data, overexpression of $SOD1^{G93A}$ sensitized $Tdp1^{-/-}$ cells to H_2O_2, while SOD1 overexpression offered some protection ($P < 0.05$; Fig. 5C). In contrast, overexpression of $SOD1^{G93A}$ had no impact on cell survival of WT cells (Fig. 5D). Having established the protective role of TDP1 in the multiple cellular systems using a variety of readouts, we then proceeded to the whole-organism level by crossing $Tdp1^{-/-}$ mice with $hSOD1^{G93A}$ mice. Our experiments suggested early embryonic lethality of the double mutant mice because we only detected three double-mutant embryos that died in utero (Table 1). However, the rarity of double mutants in the progeny is due to the proximity of $SOD1^{G93A}$ and *Tdp1* genes, which both lie on distal mouse chromosome 12 (*48*). Thus, obtaining double-mutant mice will depend on a rare recombination event between these two loci to bring the knockout Tdp1 portion and $SOD1^{G93A}$ transgene together on the same chromosome in a $SOD1^{G93A}$ parent. This is reflected in the number of $SOD1^{G93A}$; $Tdp1^{+/-}$ offspring, which was unexpectedly high (96 compared to the expected 54.5).

Finally, the role of TDP1 in protecting from oxidative-induced nuclear DNA damage could be explained either by its direct role to process 3′-oxidized DNA breaks or by an indirect role of processing TOP1-linked DNA breaks induced by H_2O_2. To ascertain the relative contribution of these two possibilities, we transiently depleted TDP1 alone or in combination with TOP1 (Fig. 5E). As expected, depletion of TOP1 reduced the level of CPT-induced TOP1 cleavage complexes (TOP1-cc), as measured by the modified alkaline comet assay (Fig. 5F). Subsequent depletion of TOP1 offered a marked protection from H_2O_2-induced cell kill ($P < 0.01$; Fig. 5, G and H). Thus, the ability of TDP1 to process nuclear TOP1-linked breaks induced by oxidative stress plays a major role in its genome maintenance function.

DISCUSSION

The proximity of the mtDNA to the ETC complexes increases its vulnerability to oxidative damage (*49*), which can trap TOP1mt and generate mtPDBs (*5*). TOP1mt-mediated mtPDBs can affect transcription in response to fluctuations in cellular energy demands (*24*, *50*, *51*). Although the repair of mtPDBs is predicted to play a key role in this response, little is known about the repair mechanisms. Here, we describe a novel mtDNA repair pathway driven by TDP1 and report its importance in maintaining mitochondrial gene transcription and bioenergetics.

Mitochondrial genetic information is tightly packed in mtDNA, and both strands are actively transcribed with one noncoding regulatory region containing the promoters for mtDNA transcription. Because mtDNA is circular, bidirectional transcription results in rapid accumulation of negative supercoils behind the RNA polymerases, which require removal by TOP1mt activity akin to the reported roles of nuclear TOP1 during transcription (*52*, *53*). Although $Top1mt^{-/-}$ MEFs accumulate more negative supercoils in mtDNA, the consequences of accumulation of TOP1mt-linked DNA breaks on mitochondrial gene transcription have not been examined. The measurement of transcript abundance by qRT-PCR generally reflects transcript turnover, which is a product of both transcription rate and transcript stability. In the context of mitochondrial genes, which are translated in organello, defective mRNA transport that can lead to transcript accumulation is ruled out. $Top1mt^{-/-}$ MEFs did not accumulate aberrant length mitochondrial transcripts (*21*), arguing against an essential role of TOP1mt in transcription elongation. Furthermore, the peak of TOP1mt binding in the noncoding regulatory region containing the two promoters strongly suggests its involvement in transcription initiation (*54*), which is the rate-limiting factor in determining transcript abundance. Thus, transcript abundance measured by qRT-PCR in our system predominantly reflects the transcription rate.

TOP1mt-cc fractionation data suggest that transient (up to 48 hours) overexpression of TOP1mt in TDP1-proficient cells in the absence of topoisomerase poisons leads to mild accumulation of mtPDBs, whereas overexpression of TOP1mt* led to a more robust increase. TOP1mt overexpression in TDP1-proficient cells led to a marked reduction of mitochondrial mRNA transcripts, which is consistent with previous reports (*21*, *55*). In contrast, overexpression of TOP1mt* resulted in higher transcript levels. Therefore, the steady-state level of TOP1mt-cc seems to positively correlate with mitochondrial transcription level. One possible explanation is through DNA damage–mediated retrograde signaling, which can up-regulate mitochondrial transcription and biogenesis (*24*, *56*–*60*). TDP1 activity is also moderately up-regulated in our cellular model, tentatively suggesting its involvement in the retrograde signaling response. It may also suggest a nuclear-mitochondrial translocation in response to mitochondrial stress, which is consistent with a previous report (*19*). These data also provide an explanation for the lack of change in mitochondrial mass following TOP1mt* expression in murine cells despite rapid mtDNA depletion (*33*), further confirming the importance of the mitochondrial TDP1 pathway to remove mtPDBs and maintain overall mitochondrial integrity.

Although translation of mitochondrial-encoded genes occurs in organello, assembly of the ETC requires importation of nuclear-encoded subunits. Given that nuclear transcription of ETC subunits is unaffected, changes in levels of the mitochondrial subunits can potentially disrupt the nuclear/mitochondrial stoichiometry, resulting in dysfunctional ETC. Intriguingly, although the levels of multiple mitochondrial transcripts are affected by the TOP1mt/TDP1 pathway, only complex III showed particular sensitivity to structural disruption. Complex III, also known as cytochrome bc_1 complex, is encoded by *CYTB* in the mitochondria, and the remaining 10 subunits are

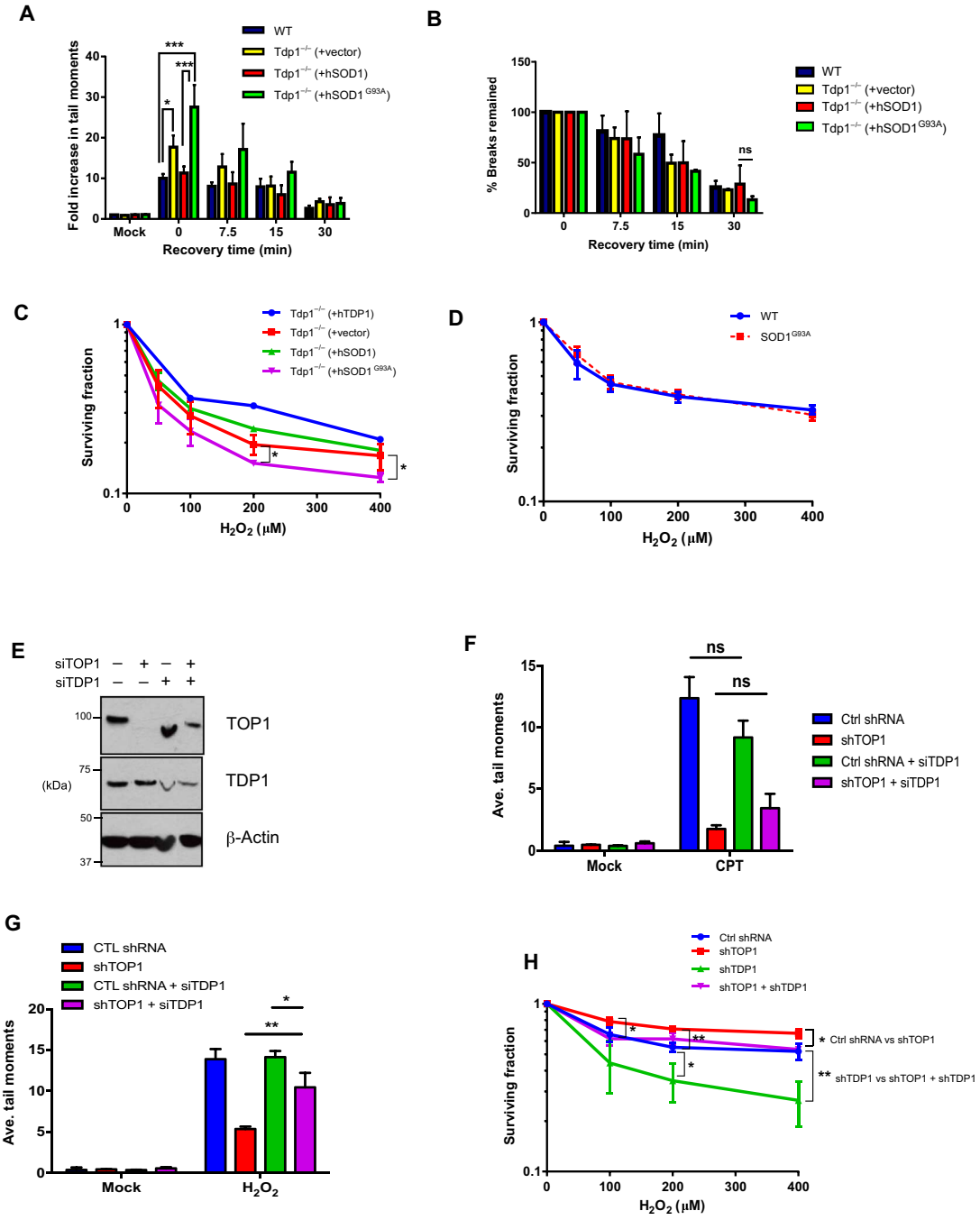

Fig. 5. TDP1 protects mammalian cells from ROS-induced chromosomal breaks. (**A**) The indicated MEF cell lines were incubated with 10 μM H_2O_2 for 10 min and then left to repair in drug-free medium at 37°C for the indicated time periods. DNA SSBs were measured using the alkaline comet assay. Average tail moments from 50 cells were quantified using the Comet Assay IV software. Data are the means of three independent experiments, and error bars represent ±1 SEM. (**B**) Repair kinetics of cells from (A) expressed as a percentage of remaining breaks over time. (**C**) Cells from (A) were treated with the indicated concentrations of H_2O_2 for 10 min on ice and then left to recover until macroscopic colonies formed. Surviving fraction was calculated by dividing the number of colonies on treated plates by the number on untreated plates. Data are the means of three independent experiments, and error bars represent ±1 SEM. (**D**) MEFs were treated with the indicated concentrations of H_2O_2 and processed as described in (C). Data are the means of three independent experiments, and error bars represent ±1 SEM. (**E**) Immunoblotting of fractionated MRC5 cell lysates from cells containing control short hairpin RNA (Ctrl shRNA) and shRNA against TOP1 (shTOP1), TDP1 (shTDP1), or both. (**F** and **G**) MRC5 cells from (E) were treated with 50 μM CPT for 1 hour (F) or 45 μM H_2O_2 for 10 min (G) and immediately lysed in buffer containing proteinase K, and TOP1-cc was quantified by the modified alkaline comet assay. Data are the means of three independent experiments, and error bars represent ±1 SEM. (**H**) MRC5 cells from (E) were treated with 10 μM H_2O_2 for 10 min on ice and then left to recover until macroscopic colonies formed. Surviving fraction was calculated by dividing the number of colonies on treated plates by the number on untreated plates. Data are the means of three independent experiments, and error bars represent ±1 SEM.

Table 1. Genotypes of live offspring of crossing hSOD1^{G93A} with different Tdp1 backgrounds. Male mice overexpressing hSOD1^{G93A} were bred with female WT mice, heterozygous for Tdp1 or homozygous for Tdp1 knockout. The live births were genotyped at 1 month postnatum.

Male parent	***Parent* hSOD1^{G93A} *Tdp1*$^{+/-}$**					
Female parent	***Sod1*$^{+/+}$ *Tdp1*$^{-/-}$**		***Sod1*$^{+/+}$ *Tdp1*$^{+/-}$**		***Sod1*$^{+/+}$ *Tdp1*$^{+/+}$**	
Offspring (no. of live births)	**Expected**	**Obtained**	**Expected**	**Obtained**	**Expected**	**Obtained**
Sod1$^{+/+}$ *Tdp1*$^{+/+}$			6.25	3	2.25	0
Sod1$^{+/+}$ *Tdp1*$^{+/-}$	54.5	6	12.5	5	2.25	4
Sod1$^{+/+}$ *Tdp1*$^{-/-}$	54.5	115	6.25	14		
hSOD1^{G93A} *Tdp1*$^{+/+}$			6.25	14	2.25	5
hSOD1^{G93A} *Tdp1*$^{+/-}$	54.5	96	12.5	12	2.25	0
hSOD1^{G93A} *Tdp1*$^{-/-}$	54.5	1*	6.25	2		
Total	218	218	50	50	9	9
Male parent	**hSOD1^{G93A}; *Tdp1*$^{+/+}$**					
Female parent	***Sod1*$^{+/+}$; *Tdp1*$^{-/-}$**		***Sod1*$^{+/+}$; *Tdp1*$^{+/-}$**		***Sod1*$^{+/+}$; *Tdp1*$^{+/+}$**	
Offspring (no. of live births)	**Expected**	**Obtained**	**Expected**	**Obtained**	**Expected**	**Obtained**
Sod1$^{+/+}$; *Tdp1*$^{+/+}$			15.25	9	7	6
Sod1$^{+/+}$; *Tdp1*$^{+/-}$	24.5	21	15.25	15		
Sod1$^{+/+}$; *Tdp1*$^{-/-}$						
hSOD1^{G93A}; *Tdp1*$^{+/+}$			15.25	23	7	8
hSOD1^{G93A}; *Tdp1*$^{+/-}$	24.5	28	15.25	14		
hSOD1^{G93A}; *Tdp1*$^{-/-}$*						
Total	49	49	61	61	14	14

*One fetus demised in utero.

all encoded in the nuclear genome. The cytochrome b subunit is the main transmembrane subunit that anchors the complex, which could explain the loss of complex III subunits in TDP1-depleted cells with or without TOP1mt* overexpression.

Because complex III plays a crucial role in handling electron transfer, dysfunction of complex III is expected to impair OXPHOS and increase ROS production. TDP1 depletion or TOP1mt* overexpression led to a reduction in OXPHOS-specific oxygen consumption, as measured by the Seahorse bioenergetics assays. Overexpression of TOP1mt* in TDP1-proficient cells resulted in severe reduction in spare respiratory capacity, indicating that the ETC function is likely to decompensate under conditions of high ATP demand. Furthermore, depletion of TDP1 in these cells partially rescued the spare respiratory capacity, suggesting that up-regulation of mitochondrial transcription has an added detrimental effect on mitochondrial bioenergetics compared to suppression of transcription, possibly through excessive consumption of ATP.

To assess the levels of ROS associated with OXPHOS dysfunction in the absence of TDP1, we used ESR spectroscopy for the first time to directly measure the level of intracellular free radicals in vertebrate cells. We used DT40 cells for these experiments because it was not possible to titrate the level of TDP1 using the inducible human system. Ultraviolet A (UVA) irradiation of DT40 and MEFs produced an ESR detectable carbon-centered adduct as the predominant radical adduct trapped by 5,5-dimethyl-1-pyrroline *N*-oxide (DMPO) (*61*). The adducts are formed intracellularly because they were detected after removal of extracellular DMPO by washing with phosphate-buffered saline (PBS), and their profile is comparable to the carbon adduct detected in UVA-irradiated isolated cell nuclei. These data are also consistent with reports showing the formation of singlet oxygen upon UVA irradiation and the photoproduction of hydrogen peroxide and superoxide anion radical (O_2^-) (*62*, *63*). We consistently detected higher levels of carbon adducts in TDP1-deficient compared to TDP1-proficient cells. The level of carbon adducts was consequently suppressed by the overexpression of SOD1, in line with previous reports (*41*). In contrast, overexpression of a toxic mutant of SOD1 (SOD1^{G93A}) led to a marked increase in carbon-centered adducts. The impact of SOD1 and SOD1^{G93A} on carbon adducts was dependent on the extent of their respective expression levels. The carbon radical adducts detected here are mobile and most likely located on exposed DNA structures such as those produced from nucleic acid fragments formed after DNA strand breaks and for which TDP1 is required for processing (*41*, *42*). Consistent with the role of TDP1 as protection against oxidative DNA damage, *Tdp1*$^{-/-}$ cells accumulated more DNA strand breaks and displayed hypersensitivity to H_2O_2. Overexpression of SOD1^{G93A} led to a further increase in strand breaks and sensitization, whereas overexpression of SOD1 offered some protection.

The cellular ESR data reported here and elegant cell-free biochemical experiments reported by the Povirk and Interthal groups demonstrate a

direct role for TDP1 in processing a wide variety of oxidized DNA fragments (*2*–*4*, *64*). However, oxidative DNA damage has also been shown to trap TOP1 on DNA (*28*, *65*, *66*), which requires TDP1 for repair (*67*). To ascertain the relative contribution of TDP1 in processing oxidative DNA breaks per se and TOP1-mediated PDBs triggered by oxidative damage, we transiently depleted TOP1 and monitored PDBs using a modification of the alkaline comet assay (*16*, *68*). TOP1 depletion suppressed CPT-induced PDBs and led to a marked protection from cell death induced by oxidative stress, suggesting that TOP1-mediated PDBs are major contributors to cell death induced by oxidative DNA breakage in situations where TDP1 is limiting.

The data reported here demonstrate a role for TDP1 in maintaining mtDNA transcription and bioenergetics, thereby controlling the level of free radical–induced DNA damage. This role is fulfilled through a functional interaction between TDP1 and both nuclear and mitochondrial TOP1. We propose that, in the mitochondria, the catalytic cycle of TOP1mt is facilitated by the removal of TOP1mt-cc by TDP1. Transcription of the mitochondrial subunits of the ETC complexes is balanced with transcription of the nuclear subunits, ensuring proper assembly of the ETC complexes. Efficient functioning of ETC complexes promotes ATP production by OXPHOS, generating a membrane potential that prevents formation of ROS (Fig. 6A). In the absence of TDP1, unrepaired TOP1mt-cc inhibits mitochondrial transcription, thereby disrupting the stoichiometry of the ETC subunits. OXPHOS efficiency is reduced, negatively affecting ATP production and increasing the formation of ROS (Fig. 6B). When excessive TOP1mt-cc is formed, for example, due to trapping by oxidized DNA lesions or TOP1mt poisons, compensatory up-regulation of TDP1 activity accelerates TOP1mt catalytic cycle and promotes mitochondrial transcription. However, without a proportional increase in nuclear transcription, misassembly of the ETC complexes takes place, which cannot be compensated for by TDP1, and thus leads to a reduction in OXPHOS and an elevation in ROS production (Fig. 6C).

The role of nuclear-encoded TDP1 to maintain mitochondrial genome stability highlights the importance of nuclear-mitochondrial interactions, which should be considered during mitochondrial donation procedures or otherwise known as three parent babies recently licensed in the UK. Notably, accumulation of nuclear PDBs is pathogenic in a number of neurological disorders such as spinocerebellar ataxia with axonal neuropathy (SCAN1) and ataxia telangiectasia (*14*). Given the high metabolic activity and energy demand of cells in the nervous system, the data reported here suggest that accumulation of mitochondrial PDBs may also be pathogenic, disrupting mitochondrial gene transcription and bioenergetics, thereby causing progressive neuronal demise. Moreover, the functional interaction between TDP1 and TOP1mt may play an important role in other clinical settings. For example, TOP1mt has been recently shown to promote liver regeneration (*23*). Pathological and drug-induced liver injuries often require partial liver transplantation, the success of which differs across individuals. This study suggests the importance of assessing TDP1 and TOP1mt genetic variants and function to improve the success of tissue regeneration. Furthermore, several cancer cell types show increased mitochondrial genomic mutations and up-regulation of nuclear-encoded enzymes that maintain mitochondrial genome stability (*69*). For example, TOP1mt transcription is up-regulated by the proto-oncogene *Myc* (*70*), offering a clinical setting where TDP1 inhibitors may be synergistic with TOP1mt poisons such as lamellarin D (*51*). On the other hand, TDP1 inhibitors should be avoided in combination with doxorubicin, which is a TOP2 poison with cardiotoxic side effects shown to be exacerbated by TOP1mt deletion (*22*, *71*). It would also be interesting to examine whether the TOP1mt$^{T554A/N558H}$ mutation is common in cancer patients because our data suggest that this mutation drives an increase in mtDNA gene transcription, which is fully dependent on TDP1. Thus, TDP1 inhibitors may offer a selective advantage in this cohort of tumors. What drives an adaptive advantage for cancer (whether it is the up-regulation or down-regulation of mtDNA transcription) remains to be clarified. Nevertheless, targeting the adaptive mechanism in cancer offers a worthy therapeutic opportunity.

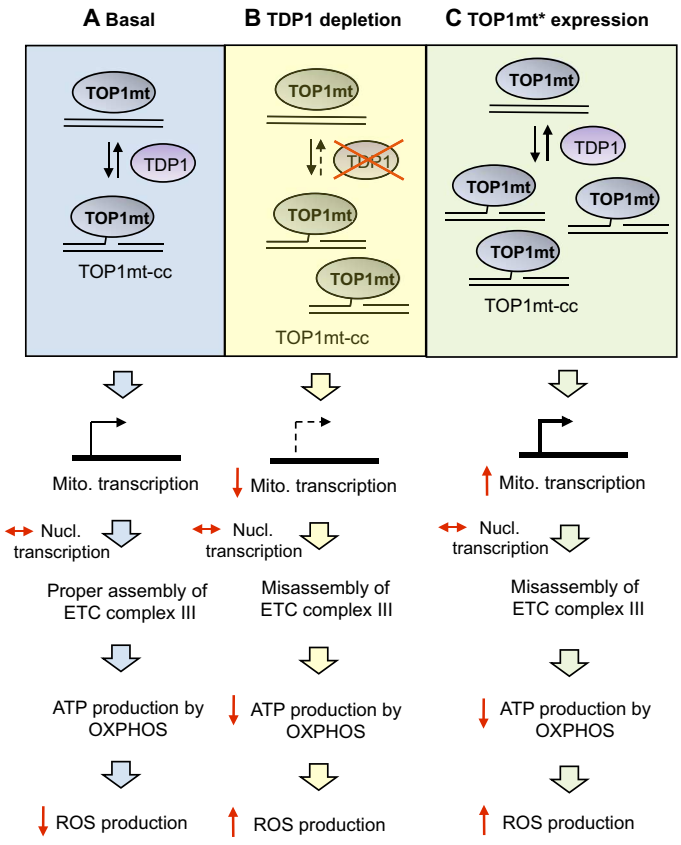

Fig. 6. Model depicting the importance of the TDP1/TOPmt repair pathway. (**A**) Under basal condition, the catalytic cycle of TOP1mt is facilitated by the removal of TOP1mt-cc by TDP1. Transcription of the mitochondrial subunits of the ETC complexes is balanced with transcription of the nuclear subunits, resulting in the proper assembly of the ETC complexes. Efficient functioning of ETC complexes promotes ATP production by OXPHOS, generating membrane potential that prevents formation of ROS. (**B**) In the absence of TDP1, TOP1mt-cc accumulate, which inhibit mitochondrial transcription without affecting transcription of the nuclear subunits, leading to misassembly of complex III. OXPHOS efficiency is reduced and ROS production is increased. (**C**) When excessive TOP1mt-cc are formed (for example, because of trapping by oxidized DNA lesions or TOP1mt poison), compensatory up-regulation of TDP1 activity accelerates TOP1mt catalytic cycle and promotes mitochondrial transcription. However, without proportional increase in nuclear transcription, misassembly of ETC complexes leads to a reduction in OXPHOS and an elevation of ROS production. Mito., mitochondrial; Nucl., nuclear.

MATERIALS AND METHODS

Cell lines and plasmids

Tdp1$^{-/-}$ MEFs were generated and genotyped as previously described (*43*). Immortalization of *Tdp1*$^{-/-}$ MEFs was achieved by continuous passage

over at least 3 months. Immortalized MEFs were maintained in Dulbecco's modified Eagle's medium (DMEM) supplemented with 15% fetal calf serum (FCS), 1× nonessential amino acids, 2 mM L-glutamine, and penicillin-streptomycin (100 U/ml). Immortalized *Tdp1*$^{-/-}$ MEFs were stably transduced with retroviral particles containing hTDP1 complementary DNA (cDNA) (NM_018319) or human WT SOD1 or SOD1^{G93A} cDNA (NM_000454) using the packaging cell line Phoenix (gift from C. Vens) transiently transfected with the plasmid pMX-PIE containing cDNAs of the relevant genes. Transduced clones were pooled and maintained in growth medium containing puromycin (1 μg/ml). *TDP1*$^{-/-}$ DT40 lymphocytes (*15*) were maintained in RPMI 1640 supplemented with 10% FCS, 1% chicken serum, 2 mM L-glutamine, 1 μM β-mercaptoethanol, and penicillin-streptomycin (100 U/ml) and grown at 39°C. MRC5 cells stably transduced with shTOP1-containing lentiviral particles, as previously described (*11*), were grown in MEM containing 10% FCS, 2 mM L-glutamine, penicillin-streptomycin (100 U/ml), and puromycin (1 μg/ml). Flp-In T-Rex 293 cells were maintained in DMEM supplemented with 15% tetracycline-free FCS, 2 mM L-glutamine, penicillin-streptomycin (100 U/ml), zeocin (100 μg/ml), and blasticidin (10 μg/ml). The two miRNA targeting regions of the TDP1 open reading frame (ORF) (5′-TGGACCATCTAGTAGTGAT-3′ and 5′-TGGTGTCTCCAGCAGTGAT-3′) were inserted into the plasmid pcDNA6.2-G.W.-EmGFP (Life Technologies) following the manufacturer's instructions. To subclone the miRNA and the EmGFP sequences into pcDNA5-FRT/TO/His (Life Technologies), restriction sites Hind III and Not I were introduced using divergent PCR with the following primers: 5′-GGCGGCAAGCTTACAAGTTTGTACAAAAAAGCAG-3′ and 5′-GGCGGCGCGGCCGCACCACTTTGTACAAGAAAGCTG-3′. To generate RNAi-resistant TDP1, silent mutations were introduced in the TDP1 ORF using the following PCR primers: 5′-GAGGT**T**CAC-**G**ATATC**A**AG**C**AG**C**GA**C**GAAAGTGAGGAAGAAAAG-3′ and 5′-CTTTC**G**TC**G**CT**G**CT**T**GATAT**C**GT**GA**ACCTCCCATAATCGC-3′. The TDP1 fragment was PCR-amplified using the following primers: 5′-aagcaggctttaaaaccATGGAACAAAAACTTATTTCTGAAGAAGATC-3′ and 5′-gcccttgctcaccatGGAGGGCACCCACATGTT-3′. In parallel, the backbone vector pcDNA5-FRT-EmGFP-pre-miRNA was amplified using the following primers: 5′-ATGGTGAGCAAGGGCGAG-3′ and 5′-GGTTTTAAAGCCTGCTTTTTTGTAC-3′. Both amplicons were gel-purified and ligated at a backbone-to-insert ratio of 1:3 using the Gibson Assembly Master Mix (New England Biolabs) according to the manufacturer's instructions. The resulting pcDNA5-FRT construct was used together with the Flp recombinase–expressing plasmid pPGKFLP to cotransfect the Flp-In T-Rex 293 cells. Single clones that have stably integrated the construct were selected with hygromycin B (100 μg/ml) for 3 weeks and maintained in media containing hygromycin B (100 μg/ml) and blasticidin (10 μg/ml). Transcription of miRNA or cDNA was induced by incubation in doxycycline (1 μg/ml) for 24 to 48 hours.

Immunoblotting

Cells were lysed in 50 mM tris, 40 mM NaCl, 2 mM $MgCl_2$, 0.5% Triton X-100, 1× protease inhibitors cocktail, and benzonase nuclease (25 U/ml) for 1 hour at 4°C. Cell lysate was cleared by centrifugation for 10 min at 4°C. Total protein concentration was determined using Bradford assay and fractionated by SDS–polyacrylamide gel electrophoresis. The following primary antibodies were used: 53BP1 (A300-273A, Bethyl Laboratories), β actin (AC-40, Sigma-Aldrich), β tubulin (ab7792, Abcam), GFP (ab290, Abcam), OXPHOS antibody cocktail (ab110411, Abcam), SOD1 (FL-154, Santa Cruz Biotechnology), TDP1 (ab4166, Abcam), TOP1 (C-21, Santa Cruz Biotechnology), VDAC1/Porin (ab15895, Abcam), and UQRC2 (ab14745, Abcam).

Detection of TOP1mt-cc by cesium chloride fractionation

Flp-In cells (2×10^7) were induced with doxycycline (1 μg/ml) for 48 hours and harvested. Mitochondria were isolated using the mitochondria isolation kit for cultured cells (89874, Thermo Fisher Scientific) following the manufacturer's instructions. Lysis of mitochondria and CsCl fractionation of TOP1mt*-cc were carried out as previously described (*72*). TOP1mt*-cc were detected using antibodies against TOP1-DNA covalent complexes (MABE1084, Millipore) or GFP (ab290, Abcam) and visualized by chemiluminescence.

Chromatin immunoprecipitation–PCR

Flp-In T-Rex 293 cells (1.5×10^7) were induced by doxycycline (1 μg/ml) for 48 hours, scraped, and then lysed in 0.5 ml of chromatin immunoprecipitation (ChIP) lysis buffer [50 mM Hepes-KOH (pH 7.5), 140 mM NaCl, 1 mM EDTA (pH 8), 1% Triton X-100, 0.1% sodium deoxycholate, 0.1% SDS, and 1× protease inhibitor] on ice for 30 min. Chromatin was sonicated to yield fragments of 200 to 300 base pairs. Ten percent of the volume of the supernatant was taken as input and snap-frozen. The remainder was diluted fourfold in radioimmunoprecipitation assay buffer [50 mM tris-HCl (pH 8), 150 mM NaCl, 2 mM EDTA (pH 8), 1% NP-40, 0.5% sodium deoxycholate, 0.1% SDS, and 1× protease inhibitors] and added to 20 μl of GFP-Trap magnetic agarose beads (ChromoTek) on a rotating carousel overnight at 4°C. The beads were then washed twice with low-salt wash buffer [0.1% SDS, 1% Triton X-100, 2 mM EDTA, 20 mM tris-HCl (pH 8), and 150 mM NaCl], twice with high-salt wash buffer [0.1% SDS, 1% Triton X-100, 2 mM EDTA, 20 mM tris-HCl (pH 8), and 500 mM NaCl], followed by one wash with lithium chloride buffer [0.25 M LiCl, 1% NP-40, 1% sodium deoxycholate, 1 mM EDTA, and 10 mM tris-HCl (pH 8)], and twice with TE buffer. The immunoprecipitated complex was then eluted from the beads in 150 μl of elution buffer (1% SDS and 100 mM $NaHCO_3$). The eluent and the input samples were then treated with RNase A and proteinase K. The DNA was purified using phenol chloroform extraction and ethanol precipitation. The pellet was resuspended in 30 μl of distilled water.

For qPCR, the input and ChIP samples were diluted 1:10, and then, 5 μl was mixed with 2.8 μl of 5 μM forward and reverse primers (5′-TACTCAAATGGGCCTGTCCT-3′ and 5′-TGGTACCCAAATCTGCTTCC-3′, respectively) and 10 μl of 2× SensiMIX SYBR Hi-ROX mastermix (QT605-05, Bioline). The mastermix was aliquoted into reaction volumes (20 μl) in duplicates using automated PCR setup workstation (CAS-1200, Corbett Robotics). The PCR reactions were carried out with thermocycling conditions of 95°C for 10 min and then 40 cycles at 90°C for 15 s, 50°C for 15 s, and 72°C for 30 s, with signal acquisition at the end of each cycle. Quantification of chromatin enrichment was calculated by percent input normalized to the mtDNA copy number in the input samples.

Mitochondrial gene transcription

Total RNA from 5×10^6 cells was extracted using Qiagen RNeasy Plus kit as per the manufacturer's instructions, which included DNase treatment of the samples, followed by reverse transcription of 5 μg of total RNA using the Tetro cDNA Synthesis Kit (Bioline). PCR primers used were as follows: GGAGCAGGAACAGGTTGAACAG (CO1 forward) and GTTGTGATGAAATTGATGGC (CO1 reverse); CCCTTACCATCAAATCAATTGGCC (CO2 forward) and

ATTGTCAACGTCAAGGAGTCGC (CO2 reverse); CTACTACAACCCTTCGCTGAC (ND1 forward) and GGATTGAGTAAACGGCTAGGC (ND1 reverse); CTGATCCTCCAAATCACCACAG (CYT-B forward) and GCGCCATTGGCGTGAAGGTA (CYT-B reverse); TAGAGGAGCCTGTTCTGTAATCGAT (RNR1 forward) and CGACCCTTAAGTTTCATAAGGGCTA (RNR1 reverse); ACATCGCTCAGACACCATG (GAPDH forward) and TGTAGTTGAGGTCAATGAAGGG (GAPDH reverse). qPCR was set up in a 20-µl reaction using 5 µl of 1:10 dilution of cDNA samples and 0.7 µM primers in 1× SensiMIX SYBR Hi-ROX mastermix (Bioline) in a Rotor-Gene 6000 qPCR machine (Corbett Research). The thermocycling conditions were 95°C for 10 min, followed by 40 cycles at 95°C for 15 s, 50°C for 15 s, and 72°C for 30 s.

Gel-shift TDP1 activity assay

Reactions were performed in reaction volumes (10 µl) containing assay buffer [25 mM Hepes (pH 8.0), 130 mM KCl, and 1 mM dithiothreitol (DTT)], 100 ng of mitochondrial lysate, and 75 nM Cy5.5-labeled substrate oligomer containing a 3′-phosphotyrosyl group, 5′-(Cy5.5) GATCTAAAAGACT(pY)-3′ (Midland Certified Reagent Company). Reactions were carried out at 37°C for 1 hour and stopped by the addition of 10 µl of loading buffer (44% deionized formamide, 2.25 mM tris-borate, 0.05 mM EDTA, 0.01% xylene cyanol, and 1% bromophenol blue). Samples were then heated at 90°C for 10 min before separation on a 20% urea SequaGel (Thermo Fisher Scientific) by gel electrophoresis at 150 V for 1 hour. Reaction products were visualized by Bio-Rad ChemiDoc MP image docking system at 635 nm, and bands were quantified using LI-COR Image Studio Lite version 5.2.

TDP1 activity assay: Fluorescence assay

In vitro 3′-tyrosyl-DNA phosphodiesterase activity of whole-cell extracts (WCE) was determined as previously described (*40*). Briefly, assays were performed in a 15-µl reaction volume containing assay buffer [50 mM tris (pH 8.0), 5 mM $MgCl_2$, 80 mM KCl, 0.05% Tween 20, and 1 mM DTT], 10 nM 13-mer substrate with a 3′-phosphotyrosyl oligonucleotide conjugated to an FITC molecule (Midland Certified Reagent Company), and 2 µl (~2 µg) of the indicated amounts of WCE. Reactions were carried out at room temperature for 10 min before quenching with a mix of 30 µl of enhancer and 2 µl of sensor (Gyrasol Technologies). Fluorescence intensity was measured using a BMG Labtech PHERAstar plate reader at an excitation wavelength (λ_{ex}) of 490 nm and an emission wavelength (λ_{em}) of 520 nm. Recombinant hTDP1 (6.5 pM) diluted in assay buffer was used as a 3′-tyrosyl-DNA phosphodiesterase activity control.

Mitochondrial bioenergetic profiling by Seahorse Bioanalyzer

Flp-In T-Rex 293 cells were induced in doxycycline (1 µg/ml) for 24 hours and then seeded (6×10^4 cells per well) in a 24-well Seahorse cell culture plate (100777-004, Seahorse Bioscience) precoated with Cell-Tak cell adhesive in 575 µl of XF assay media (101022-100, Seahorse Bioscience) supplemented with glucose (4.5 mg/ml), 2 mM L-glutamine, and 1× sodium pyruvate. Cells were incubated at 37°C with atmospheric CO_2 for 1 hour. A XF24 flux plate prehydrated in calibrant buffer was loaded with 10 µM oligomycin, FCCP, and rotenone (final concentration, 1 µM) diluted in the supplemented XF assay medium. Three basal readings were taken (3 min each), followed by addition of oligomycin, FCCP, and rotenone, with three readings taken after the addition of each drug. Cells were washed with PBS once and then incubated in DMEM containing Hoechst 33342 (25 µg/ml) at 37°C for 30 min. The images were captured with an IN Cell Analyzer 6000 cell imaging system (GE Healthcare), and the nuclei number in each well was quantified using the IN Cell Developer software (GE Healthcare).

ESR spectroscopy

ESR experiments were undertaken using a JEOL FA100 Spectrometer with the following typical settings: microwave power, 20 mW; modulation, 0.2 mT; signal amplitude, 2×10^3; sweep time, 5 s with repeated scanning (25 scans). For irradiations, a 300-W Oriel Xenon lamp (ozone-free) was used, and radiation >260 nm passed through a water filter to remove infrared radiation and then two optical glass filters (4- to 5-mm-thick WG320 Schott filter, UQG Optics Ltd.) to filter UVB/UVC. In studies involving MEFs, an irradiance of 40 mW/cm^2 (UVA-visible light) was measured at the distance of the sample from the fiber-optic probe using an ILT1400-A Radiometer photometer equipped with a thermopile detector measuring radiation over the full spectral range. In studies of DT40 cells, a UVA-visible irradiance of 25 mW/cm^2 was measured at the position of the sample. Using a 1:7 ratio of UVA to visible light from solar simulator spectral irradiance data (Oriel Instruments Light Sources Catalog), it was estimated that the UVA irradiance at the position of the cells in the spectrometer was approximately 3.1 to 5 mW/cm^2 of UVA and comparable to sunshine in southern latitudes. For DT40 cells, 60×10^6 cells were harvested and then incubated with the spin-trapping agent DMPO (0.9 M in PBS) for 60 min at room temperature. Cells were then washed with 10 ml of PBS, centrifuged, resuspended in 187 µl of PBS (320,000 cells/µl), and loaded in the ESR quartz cell. For MEFs, 10^7 cells were harvested, and DMPO-treated cells were resuspended in 125 µl of PBS (80,000 cells/µl). All cells were then exposed to UVA-visible light irradiation for 30 min in situ and free radical adducts were measured in real time. The ESR profile consisted of nucleic acid–derived radicals (R.H., in preparation), and quantification of the UVA-induced carbon radical was conducted by integration of the low-field signal of the carbon adduct relative to the Mn line (of the internal manganese reference sample in the spectrometer) in line with previous ESR quantifications (*73*).

Alkaline comet assays and the modified alkaline comet assays

Immortalized MEFs or Flp-In T-Rex 293 cells (~3×10^5 cells per sample) were suspended in normal growth media (for IR and CPT treatments) or cold PBS (for H_2O_2 treatment) and subjected to 20-gray gamma ray, 14 µM CPT for 1 hour at 37°C, or 10 µM H_2O_2 for 10 min on ice, and then incubated in normal growth media at 37°C for the indicated repair time. Repair was stopped by placing cells on ice and replacing media with cold PBS. Approximately 5000 cells were mixed with equal volumes of PBS and 1.2% type VII agarose at 42°C, plated on frosted microscope slides precoated with 0.6% agarose, and chilled until set. Cells were then lysed in 2.5 M NaCl, 10 mM tris-HCl, 100 mM EDTA (pH 8), 1% Triton X-100, and 1% dimethyl sulfoxide (DMSO) (pH 10) at 4°C for 1 hour and washed twice with cold distilled water. Slides were equilibrated in alkaline electrophoresis buffer (50 mM NaOH, 1 mM EDTA, and 1% DMSO) for 45 min and then subjected to electrophoresis at 12 V (100 mA) for 25 min. Quantification of DNA breaks was performed using Comet Assay IV software, counting 50 cells per sample. The modified alkaline comet assay detects PDBs and was conducted as previously described (*16*). Briefly, proteinase K (0.8 mg/ml) was added to the cells immediately after CPT or H_2O_2 treatment. Cells were then mixed with equal volumes of PBS and 1.2% type VII agarose

and plated on frosted microscope slides precoated with 0.6% agarose. Lysis was performed in the presence of proteinase K (0.4 mg/ml) at 37°C for 3 hours. Slides were then processed as described above.

Clonogenic survival assay

MEFs were seeded at 2000 to 10,000 cells in 10-cm petri dish and incubated overnight in normal growth media. Cells were incubated with CPT for 1 hour at 37°C and exposed to x-ray (250 kV at 12 mA) or H_2O_2 (10 min on ice) at the indicated doses. Cells treated with CPT or H_2O_2 were washed twice with PBS and grown in drug-free media for 7 days. Cells were then fixed with 80% ethanol for 15 min and stained with 1% methylene blue. Surviving fraction was calculated by dividing the number of colonies normalized to cell numbers on treated plates by the number of colonies normalized to cell numbers on untreated plates. The average ±1 SEM was calculated from three independent biological repeats. MRC5 cells with TOP1 or TDP1 shRNA knockdown were seeded at 500 to 2000 cells in 10-cm dishes and incubated at 37°C for 5 hours or until they became adherent. Cells were then treated with H_2O_2 for 10 min on ice at the indicated doses. Cells were washed twice with PBS and grown in drug-free media for 7 days. Cells were then fixed with 80% ethanol for 15 min and stained with 1% methylene blue. Percentage of colony survival was normalized to mock-treated sample.

Cell viability assay

Flp-In T-Rex 293 cells were induced with doxycycline (1 μg/ml) for 24 hours, seeded at densities of 2000 to 20,000 cells per 100 μl, and treated with the indicated concentrations of CPT in the absence of doxycycline for 72 hours. Cell viability was measured using the CellTiter-Blue kit (Promega). The CellTiter-Blue reagent (20 μl) was mixed with the cells and incubated at 37°C for 1 hour. Fluorescence intensity was measured at an excitation/emission wavelength of 544/590 ± 10 nm using a FLUOstar Omega plate reader (BMG Labtech). Viability of untreated cells was set to 1, and error bars represent SE from three independent biological repeats.

Genotyping

Tdp1$^{-/-}$ mice were generated as previously described (*43*). *Tdp1*$^{+/-}$ mice were mated with SOD1^{G93A} mice (*74*) to generate *Tdp1*$^{+/-}$ *SOD1*^{G93A} males, which were backcrossed with *Tdp1*$^{+/+}$, *Tdp1*$^{+/-}$, or *Tdp1*$^{-/-}$ females. Genotyping of adult mice was conducted using tail biopsies, which were digested in 100 μl of 25 mM NaOH at 95°C for 2 hours and diluted with 400 μl of 10 mM tris-HCl (pH 8). Lysate (5 μl) was used as template in PCR reactions, as previously described (*74*). Genotyping for SOD1^{G93A} was performed using primers 5′-CATCAGCCCTAATCCATCTGA-3′ and 5′-CGCGACTAACAATCAAAGTGA-3′. All animals were housed and maintained in accordance with the institutional animal care and ethical committee at the University of Sussex.

Statistical analyses

For the survival assays, the mean and SEs were calculated from at least three biological repeat experiments consisting of three technical replicates at each treatment condition. The *P* values of samples from each time point or concentration were analyzed by two-tailed paired Student's *t* test. For the alkaline comet assays, the mean and SEs were calculated from at least three biological repeat experiments consisting of tail moment scores from 50 cells. For the H_2O_2 comet assay, the mean comet tail moments of all samples were normalized to the mock-treated WT sample. The *P* values of samples from each time point or concentration were analyzed by two-tailed paired Student's *t* test. For qRT-PCR experiments, a standard curve was generated from pooled cDNAs from all cell lines serially diluted over 10-, 100-, and 1000-fold. Relative quantification of the Ct (threshold cycle) values of all samples was extrapolated from the standard curve and normalized against GAPDH values. The normalized values were then expressed as fold change relative to the miScr cell line. The mean values and SEs were calculated from three biological repeat experiments. The *P* values were calculated using two-way analysis of variance (ANOVA) with Bonferroni post hoc test using GraphPad Prism version 6 (GraphPad Software).

SUPPLEMENTARY MATERIALS

Supplementary material for this article is available at http://advances.sciencemag.org/cgi/content/full/3/4/e1602506/DC1

fig. S1. The generation of an inducible TDP1 knockdown system in Flp-In T-Rex 293 cells.
fig. S2. Quantification of TOP1mt-cc in TOP1mt-overexpressing cells.
fig. S3. TDP1 depletion had no impact on the expression of the nuclear-encoded complex II subunit.
fig. S4. TDP1 depletion or TOP1mt* expression does not affect uncoupled respiration (proton leak).

REFERENCES AND NOTES

1. K. Akopiants, S. Mohapatra, V. Menon, T. Zhou, K. Valerie, L. F. Povirk, Tracking the processing of damaged DNA double-strand break ends by ligation-mediated PCR: Increased persistence of 3′-phosphoglycolate termini in SCAN1 cells. *Nucleic Acids Res.* **42**, 3125–3137 (2014).
2. T. Zhou, K. Akopiants, S. Mohapatra, P.-S. Lin, K. Valerie, D. A. Ramsden, S. P. Lees-Miller, L. F. Povirk, Tyrosyl-DNA phosphodiesterase and the repair of 3′-phosphoglycolate-terminated DNA double-strand breaks. *DNA Repair* **8**, 901–911 (2009).
3. T. Zhou, J. W. Lee, H. Tatavarthi, J. R. Lupski, K. Valerie, L. F. Povirk, Deficiency in 3′-phosphoglycolate processing in human cells with a hereditary mutation in tyrosyl-DNA phosphodiesterase (TDP1). *Nucleic Acids Res.* **33**, 289–297 (2005).
4. K. V. Inamdar, J. J. Pouliot, T. Zhou, S. P. Lees-Miller, A. Rasouli-Nia, L. F. Povirk, Conversion of phosphoglycolate to phosphate termini on 3′ overhangs of DNA double strand breaks by the human tyrosyl-DNA phosphodiesterase hTdp1. *J. Biol. Chem.* **277**, 27162–27168 (2002).
5. M. E. Ashour, R. Atteya, S. F. El-Khamisy, Topoisomerase-mediated chromosomal break repair: An emerging player in many games. *Nat. Rev. Cancer* **15**, 137–151 (2015).
6. Y. Pommier, S.-y. N. Huang, R. Gao, B. B. Das, J. Murai, C. Marchand, Tyrosyl-DNA-phosphodiesterases (TDP1 and TDP2). *DNA Repair* **19**, 114–129 (2014).
7. N. A. Lebedeva, N. I. Rechkunova, S. F. El-Khamisy, O. I. Lavrik, Tyrosyl-DNA phosphodiesterase 1 initiates repair of apurinic/apyrimidinic sites. *Biochimie* **94**, 1749–1753 (2012).
8. M. Alagoz, D. C. Gilbert, S. El-Khamisy, A. J. Chalmers, DNA repair and resistance to topoisomerase I inhibitors: Mechanisms, biomarkers and therapeutic targets. *Curr. Med. Chem.* **19**, 3874–3885 (2012).
9. C. Meisenberg, D. C. Gilbert, A. Chalmers, V. Haley, S. Gollins, S. E. Ward, S. F. El-Khamisy, Clinical and cellular roles for TDP1 and TOP1 in modulating colorectal cancer response to irinotecan. *Mol. Cancer Ther.* **14**, 575–585 (2014).
10. C. Meisenberg, S. E. Ward, P. Schmid, S. F. El-Khamisy, TDP1/TOP1 ratio as a promising indicator for the response of small cell lung cancer to topotecan. *J. Cancer Sci. Ther.* **6**, 258–267 (2014).
11. M. Alagoz, O. S. Wells, S. F. El-Khamisy, TDP1 deficiency sensitizes human cells to base damage via distinct topoisomerase I and PARP mechanisms with potential applications for cancer therapy. *Nucleic Acids Res.* **42**, 3089–3103 (2014).
12. B. B. Das, S.-y. N. Huang, J. Murai, I. Rehman, J.-C. Amé, S. Sengupta, S. K. Das, P. Majumdar, H. Zhang, D. Biard, H. K. Majumder, V. Schreiber, Y. Pommier, PARP1–TDP1 coupling for the repair of topoisomerase I–induced DNA damage. *Nucleic Acids Res.* **42**, 4435–4449 (2014).
13. J. Murai, S.-y. N. Huang, B. B. Das, T. S. Dexheimer, S. Takeda, Y. Pommier, Tyrosyl-DNA phosphodiesterase 1 (TDP1) repairs DNA damage induced by topoisomerases I and II and base alkylation in vertebrate cells. *J. Biol. Chem.* **287**, 12848–12857 (2012).
14. S. F. El-Khamisy, To live or to die: A matter of processing damaged DNA termini in neurons. *EMBO Mol. Med.* **3**, 78–88 (2011).

15. Z. Zeng, A. Sharma, L. Ju, J. Murai, L. Umans, L. Vermeire, Y. Pommier, S. Takeda, D. Huylebroeck, K. W. Caldecott, S. F. El-Khamisy, TDP2 promotes repair of topoisomerase I-mediated DNA damage in the absence of TDP1. *Nucleic Acids Res.* **40**, 8371–8380 (2012).
16. M. Alagoz, S.-C. Chiang, A. Sharma, S. F. El-Khamisy, ATM deficiency results in accumulation of DNA-topoisomerase I covalent intermediates in neural cells. *PLOS ONE* **8**, e58239 (2013).
17. D. C. Gilbert, A. J. Chalmers, S. F. El-Khamisy, Topoisomerase I inhibition in colorectal cancer: Biomarkers and therapeutic targets. *Br. J. Cancer* **106**, 18–24 (2012).
18. B. B. Das, T. S. Dexheimer, K. Maddali, Y. Pommier, Role of tyrosyl-DNA phosphodiesterase (TDP1) in mitochondria. *Proc. Natl. Acad. Sci. U.S.A.* **107**, 19790–19795 (2010).
19. H. K. Fam, M. K. Chowdhury, C. Walton, K. Choi, C. F. Boerkoel, G. Hendson, Expression profile and mitochondrial colocalization of Tdp1 in peripheral human tissues. *J. Mol. Histol.* **44**, 481–494 (2013).
20. B. Banerjee, A. Roy, N. Sen, H. K. Majumder, A tyrosyl DNA phosphodiesterase 1 from kinetoplastid parasite *Leishmania donovani* (*Ld*Tdp1) capable of removing topo I-DNA covalent complexes. *Mol. Microbiol.* **78**, 119–137 (2010).
21. S. Sobek, I. Dalla Rosa, Y. Pommier, B. Bornholz, F. Kalfalah, H. Zhang, R. J. Wiesner, J.-C. von Kleist-Retzow, F. Hillebrand, H. Schaal, C. Mielke, M. O. Christensen, F. Boege, Negative regulation of mitochondrial transcription by mitochondrial topoisomerase I. *Nucleic Acids Res.* **41**, 9848–9857 (2013).
22. S. Khiati, I. Dalla Rosa, C. Sourbier, X. Ma, V. A. Rao, L. M. Neckers, H. Zhang, Y. Pommier, Mitochondrial topoisomerase I (Top1mt) is a novel limiting factor of doxorubicin cardiotoxicity. *Clin. Cancer Res.* **20**, 4873–4881 (2014).
23. S. Khiati, S. A. Baechler, V. M. Factor, H. Zhang, S.-y. N. Huang, I. Dalla Rosa, C. Sourbier, L. Neckers, S. S. Thorgeirsson, Y. Pommier, Lack of mitochondrial topoisomerase I (*TOP1mt*) impairs liver regeneration. *Proc. Natl. Acad. Sci. U.S.A.* **112**, 11282–11287 (2015).
24. C. Douarre, C. Sourbier, I. Dalla Rosa, B. Brata Das, C. E. Redon, H. Zhang, L. Neckers, Y. Pommier, Mitochondrial topoisomerase I is critical for mitochondrial integrity and cellular energy metabolism. *PLOS ONE* **7**, e41094 (2012).
25. H. Zhang, J. M. Barceló, B. Lee, G. Kohlhagen, D. B. Zimonjic, N. C. Popescu, Y. Pommier, Human mitochondrial topoisomerase I. *Proc. Natl. Acad. Sci. U.S.A.* **98**, 10608–10613 (2001).
26. Y. Seol, H. Zhang, Y. Pommier, K. C. Neuman, A kinetic clutch governs religation by type IB topoisomerases and determines camptothecin sensitivity. *Proc. Natl. Acad. Sci. U.S.A.* **109**, 16125–16130 (2012).
27. D. A. Koster, V. Croquette, C. Dekker, S. Shuman, N. H. Dekker, Friction and torque govern the relaxation of DNA supercoils by eukaryotic topoisomerase IB. *Nature* **434**, 671–674 (2005).
28. P. Pourquier, L.-M. Ueng, J. Fertala, D. Wang, H.-J. Park, J. M. Essigmann, M.-A. Bjornsti, Y. Pommier, Induction of reversible complexes between eukaryotic DNA topoisomerase I and DNA-containing oxidative base damages. 7,8-Dihydro-8-oxoguanine and 5-hydroxycytosine. *J. Biol. Chem.* **274**, 8516–8523 (1999).
29. P. Pourquier, Y. Pommier, Topoisomerase I-mediated DNA damage. *Adv. Cancer Res.* **80**, 189–216 (2001).
30. P. Daroui, S. D. Desai, T.-K. Li, A. A. Liu, L. F. Liu, Hydrogen peroxide induces topoisomerase I-mediated DNA damage and cell death. *J. Biol. Chem.* **279**, 14587–14594 (2004).
31. Y. Pommier, J. M. Barcelo, V. A. Rao, O. Sordet, A. G. Jobson, L. Thibaut, Z.-H. Miao, J. A. Seiler, H. Zhang, C. Marchand, K. Agama, J. L. Nitiss, C. Redon, Repair of topoisomerase I-mediated DNA damage. *Prog. Nucleic Acid Res. Mol. Biol.* **81**, 179–229 (2006).
32. S. Medikayala, B. Piteo, X. Zhao, J. G. Edwards, Chronically elevated glucose compromises myocardial mitochondrial DNA integrity by alteration of mitochondrial topoisomerase function. *Am. J. Physiol. Cell Physiol.* **300**, C338–C348 (2011).
33. I. Dalla Rosa, S.-y. N. Huang, K. Agama, S. Khiati, H. Zhang, Y. Pommier, Mapping topoisomerase sites in mitochondrial DNA with a poisonous mitochondrial topoisomerase I (Top1mt). *J. Biol. Chem.* **289**, 18595–18602 (2014).
34. K. W. Caldecott, Single-strand break repair and genetic disease. *Nat. Rev. Genet.* **9**, 619–631 (2008).
35. C. Meisenberg, M. E. Ashour, L. El-Shafie, C. Liao, A. Hodgson, A. Pilborough, S. A. Khurram, J. A. Downs, S. E. Ward, S. F. El-Khamisy, Epigenetic changes in histone acetylation underpin resistance to the topoisomerase I inhibitor irinotecan. *Nucleic Acids Res.* **45**, 1159–1176 (2016).
36. W. Elsayed, L. El-Shafie, M. K. Hassan, M. A. Farag, S. F. El-Khamisy, Isoeugenol is a selective potentiator of camptothecin cytotoxicity in vertebrate cells lacking TDP1. *Sci. Rep.* **6**, 26626 (2016).
37. T. G. Burke, Z. Mi, The structural basis of camptothecin interactions with human serum albumin: Impact on drug stability. *J. Med. Chem.* **37**, 40–46 (1994).
38. A. G. Patel, K. S. Flatten, K. L. Peterson, T. G. Beito, P. A. Schneider, A. L. Perkins, D. A. Harki, S. H. Kaufmann, Immunodetection of human topoisomerase I-DNA covalent complexes. *Nucleic Acids Res.* **44**, 2816–2826 (2016).
39. M. Woś, J. Szczepanowska, S. Pikula, A. Tylki-Szymańska, K. Zabłocki, J. Bandorowicz-Pikuła, Mitochondrial dysfunction in fibroblasts derived from patients with Niemann-Pick type C disease. *Arch. Biochem. Biophys.* **593**, 50–59 (2016).
40. S. Walker, C. Meisenberg, R. A. Bibby, T. Askwith, G. Williams, F. H. Rininsland, L. H. Pearl, A. W. Oliver, S. El-Khamisy, S. Ward, J. R. Atack, Development of an oligonucleotide-based fluorescence assay for the identification of tyrosyl-DNA phosphodiesterase 1 (TDP1) inhibitors. *Anal. Biochem.* **454**, 17–22 (2014).
41. R. Haywood, F. Rogge, M. Lee, Protein, lipid, and DNA radicals to measure skin UVA damage and modulation by melanin. *Free Radic. Biol. Med.* **44**, 990–1000 (2008).
42. R. Haywood, C. Andrady, N. Kassouf, N. Sheppard, Intensity-dependent direct solar radiation- and UVA-induced radical damage to human skin and DNA, lipids and proteins. *Photochem. Photobiol.* **87**, 117–130 (2011).
43. S. Katyal, S. F. El-Khamisy, H. R. Russell, Y. Li, L. Ju, K. W. Caldecott, P. J. McKinnon, TDP1 facilitates chromosomal single-strand break repair in neurons and is neuroprotective in vivo. *EMBO J.* **26**, 4720–4731 (2007).
44. M. E. Gurney, H. Pu, A. Y. Chiu, M. C. Dal Canto, C. Y. Polchow, D. D. Alexander, J. Caliendo, A. Hentati, Y. W. Kwon, H.-X. Deng, W. Chen, P. Zhai, R. L. Sufit, T. Siddique, Motor neuron degeneration in mice that express a human Cu,Zn superoxide dismutase mutation. *Science* **264**, 1772–1775 (1994).
45. F. Haber, J. Weiss, The catalytic decomposition of hydrogen peroxide by iron salts. *Proc. R. Soc. A* **147**, 332–351 (1934).
46. S. Goldstein, D. Meyerstein, G. Czapski, The Fenton reagents. *Free Radic. Biol. Med.* **15**, 435–445 (1993).
47. M. Wiedau-Pazos, J. J. Goto, S. Rabizadeh, E. B. Gralla, J. A. Roe, M. K. Lee, J. S. Valentine, D. E. Bredesen, Altered reactivity of superoxide dismutase in familial amyotrophic lateral sclerosis. *Science* **271**, 515–518 (1996).
48. F. Achilli, S. Boyle, D. Kieran, R. Chia, M. Hafezparast, J. E. Martin, G. Schiavo, L. Greensmith, W. Bickmore, E. M. Fisher, The SOD1 transgene in the G93A mouse model of amyotrophic lateral sclerosis lies on distal mouse chromosome 12. *Amyotroph. Lateral Scler. Other Motor Neuron Disord.* **6**, 111–114 (2005).
49. F. M. Yakes, B. Van Houten, Mitochondrial DNA damage is more extensive and persists longer than nuclear DNA damage in human cells following oxidative stress. *Proc. Natl. Acad. Sci. U.S.A.* **94**, 514–519 (1997).
50. C. Ballot, J. Kluza, S. Lancel, A. Martoriati, S. M. Hassoun, L. Mortier, J.-C. Vienne, G. Briand, P. Formstecher, C. Bailly, R. Nevière, P. Marchetti, Inhibition of mitochondrial respiration mediates apoptosis induced by the anti-tumoral alkaloid lamellarin D. *Apoptosis* **15**, 769–781 (2010).
51. S. Khiati, Y. Seol, K. Agama, I. Dalla Rosa, S. Agrawal, K. Fesen, H. Zhang, K. C. Neuman, Y. Pommier, Poisoning of mitochondrial topoisomerase I by lamellarin D. *Mol. Pharmacol.* **86**, 193–199 (2014).
52. M. Drolet, X. Bi, L. F. Liu, Hypernegative supercoiling of the DNA template during transcription elongation in vitro. *J. Biol. Chem.* **269**, 2068–2074 (1994).
53. S. L. French, M. L. Sikes, R. D. Hontz, Y. N. Osheim, T. E. Lambert, A. El Hage, M. M. Smith, D. Tollervey, J. S. Smith, A. L. Beyer, Distinguishing the roles of Topoisomerases I and II in relief of transcription-induced torsional stress in yeast rRNA genes. *Mol. Cell. Biol.* **31**, 482–494 (2011).
54. H. Zhang, Y. Pommier, Mitochondrial topoisomerase I sites in the regulatory D-loop region of mitochondrial DNA. *Biochemistry* **47**, 11196–11203 (2008).
55. J. E. Kolesar, C. Y. Wang, Y. V. Taguchi, S.-H. Chou, B. A. Kaufman, Two-dimensional intact mitochondrial DNA agarose electrophoresis reveals the structural complexity of the mammalian mitochondrial genome. *Nucleic Acids Res.* **41**, e58 (2013).
56. R. C. Scarpulla, Nuclear control of respiratory gene expression in mammalian cells. *J. Cell. Biochem.* **97**, 673–683 (2006).
57. B. Gong, Q. Chen, A. Almasan, Ionizing radiation stimulates mitochondrial gene expression and activity. *Radiat. Res.* **150**, 505–512 (1998).
58. H.-C. Lee, P.-H. Yin, C.-Y. Lu, C.-W. Chi, Y.-H. Wei, Increase of mitochondria and mitochondrial DNA in response to oxidative stress in human cells. *Biochem. J.* **348**, 425–432 (2000).
59. J. Kluza, P. Marchetti, M.-A. Gallego, S. Lancel, C. Fournier, A. Loyens, J.-C. Beauvillain, C. Bailly, Mitochondrial proliferation during apoptosis induced by anticancer agents: Effects of doxorubicin and mitoxantrone on cancer and cardiac cells. *Oncogene* **23**, 7018–7030 (2004).
60. X. Fu, S. Wan, Y. L. Lyu, L. F. Liu, H. Qi, Etoposide induces ATM-dependent mitochondrial biogenesis through AMPK activation. *PLOS ONE* **3**, e2009 (2008).
61. C. Nishizawa, K. Takeshita, J.-i. Ueda, M. Mizuno, K. T. Suzuki, T. Ozawa, Hydroxyl radical generation caused by the reaction of singlet oxygen with a spin trap, DMPO, increases significantly in the presence of biological reductants. *Free Radic. Res.* **38**, 385–392 (2004).
62. G. F. Vile, R. M. Tyrrell, UVA radiation-induced oxidative damage to lipids and proteins in vitro and in human skin fibroblasts is dependent on iron and singlet oxygen. *Free Radic. Biol. Med.* **18**, 721–730 (1995).

63. J. Taira, K. Mimura, T. Yoneya, A. Hagi, A. Murakami, K. Makino, Hydroxyl radical formation by UV-irradiated epidermal cells. *J. Biochem.* **111**, 693–695 (1992).
64. H. Interthal, H. J. Chen, J. J. Champoux, Human Tdp1 cleaves a broad spectrum of substrates, including phosphoamide linkages. *J. Biol. Chem.* **280**, 36518–36528 (2005).
65. D.-T. T. Lesher, Y. Pommier, L. Stewart, M. R. Redinbo, 8-Oxoguanine rearranges the active site of human topoisomerase I. *Proc. Natl. Acad. Sci. U.S.A.* **99**, 12102–12107 (2002).
66. O. Sordet, Q. A. Khan, Y. Pommier, Apoptotic topoisomerase I-DNA complexes induced by oxygen radicals and mitochondrial dysfunction. *Cell Cycle* **3**, 1095–1097 (2004).
67. S. F. El-Khamisy, G. M. Saifi, M. Weinfeld, F. Johansson, T. Helleday, J. R. Lupski, K. W. Caldecott, Defective DNA single-strand break repair in spinocerebellar ataxia with axonal neuropathy-1. *Nature* **434**, 108–113 (2005).
68. L. Carlessi, E. Fusar Poli, G. Bechi, M. Mantegazza, B. Pascucci, L. Narciso, E. Dogliotti, C. Sala, C. Verpelli, D. Lecis, D. Delia, Functional and molecular defects of hiPSC-derived neurons from patients with ATM deficiency. *Cell Death Dis.* **5**, e1342 (2014).
69. J. Lu, L. K. Sharma, Y. Bai, Implications of mitochondrial DNA mutations and mitochondrial dysfunction in tumorigenesis. *Cell Res.* **19**, 802–815 (2009).
70. F. Li, Y. Wang, K. I. Zeller, J. J. Potter, D. R. Wonsey, K. A. O'Donnell, J.-w. Kim, J. T. Yustein, L. A. Lee, C. V. Dang, Myc stimulates nuclearly encoded mitochondrial genes and mitochondrial biogenesis. *Mol. Cell. Biol.* **25**, 6225–6234 (2005).
71. R. Atteya, M. E. Ashour, E. E. Ibrahim, M. A. Farag, S. F. El-Khamisy, Chemical screening identifies the β-Carboline alkaloid harmine to be synergistically lethal with doxorubicin. *Mech. Ageing Dev.* **161**, 141–148 (2016).
72. E. Hartsuiker, Detection of covalent DNA-bound Spo11 and topoisomerase complexes. *Methods Mol. Biol.* **745**, 65–77 (2011).
73. R. Haywood, A. Volkov, C. Andrady, R. Sayer, Measuring sunscreen protection against solar-simulated radiation-induced structural radical damage to skin using ESR/spin trapping: Development of an ex vivo test method. *Free Radic. Res.* **46**, 265–275 (2012).
74. J. Carroll, T. K. W. Page, S.-C. Chiang, B. Kalmar, D. Bode, L. Greensmith, P. J. McKinnon, J. R. Thorpe, M. Hafezparast, S. F. El-Khamisy, Expression of a pathogenic mutation of SOD1 sensitizes aprataxin-deficient cells and mice to oxidative stress and triggers hallmarks of premature ageing. *Hum. Mol. Genet.* **24**, 828–840 (2015).

Acknowledgment: We thank R. Lightowlers for advice on mitochondrial experiments and useful discussions, H. Mortiboys for help with the Seahorse experiments, L. Ju for assistance with the mouse experiments, and members of the El-Khamisy laboratory for useful discussions. We also acknowledge N. El-Khamisy for the help in generating the cover artwork. **Funding:** This work was funded by a Wellcome Trust Investigator award (103844), a Lister Institute of Preventative Medicine fellowship, and a European Union British Council award to S.F.E.-K. R.H. was supported by a Cancer Research U.K. grant (C1474/A10235) P.J.M. was funded by the NIH (NS-37956, CA-21765). **Author contributions:** S.-C.C. generated the model cell lines and conducted the mitochondrial TOP1-cc purification, quantitation, mitochondrial gene expression, bioenergetics, and DNA repair and survival assays. M.M. helped with the mitochondrial assays. N.K. conducted the ESR experiments. M.H. provided the $SOD1^{G93A}$ mouse model. P.J.M. provided the $Tdp1^{-/-}$ mouse model. R.H. supervised the ESR experiments. S.F.E.-K. conceived and managed the project and wrote the manuscript. All authors edited the manuscript. **Competing interests:** The authors declare that they have no competing interests. **Data and materials availability:** All data needed to evaluate the conclusions in the paper are present in the paper and/or the Supplementary Materials. Additional data related to this paper may be requested from the authors.

Submitted 12 October 2016
Accepted 2 March 2017
Published 28 April 2017
10.1126/sciadv.1602506

Citation: S.-C. Chiang, M. Meagher, N. Kassouf, M. Hafezparast, P. J. McKinnon, R. Haywood, S. F. El-Khamisy, Mitochondrial protein-linked DNA breaks perturb mitochondrial gene transcription and trigger free radical–induced DNA damage. *Sci. Adv.* **3**, e1602506 (2017).